DEVELOPMENTAL BIOLOGY

A global gene regulatory program and its region-specific regulator partition neurons into commissural and ipsilateral projection types

Aki Masuda[1], Kazuhiko Nishida[2], Rieko Ajima[1]†, Yumiko Saga[1], Marah Bakhtan[3], Avihu Klar[3], Tatsumi Hirata[1], Yan Zhu[1]*

Understanding the genetic programs that drive neuronal diversification into classes and subclasses is key to understand nervous system development. All neurons can be classified into two types: commissural and ipsilateral, based on whether their axons cross the midline or not. However, the gene regulatory program underlying this binary division is poorly understood. We identified a pair of basic helix-loop-helix transcription factors, Nhlh1 and Nhlh2, as a global transcriptional mechanism that controls the laterality of all floor plate–crossing commissural axons in mice. Mechanistically, Nhlh1/2 play an essential role in the expression of Robo3, the key guidance molecule for commissural axon projections. This genetic program appears to be evolutionarily conserved in chick. We further discovered that Isl1, primarily expressed in ipsilateral neurons within neural tubes, negatively regulates the Robo3 induction by Nhlh1/2. Our findings elucidate a gene regulatory strategy where a conserved global mechanism intersects with neuron class–specific regulators to control the partitioning of neurons based on axon laterality.

INTRODUCTION

Understanding the genetic programs that drive neuronal diversification into different classes and subclasses is a fundamental question in nervous system development. One well-understood strategy for classification of neurons is based on lineages derived from spatially, temporally, or molecularly defined progenitor domains (*1*–*3*). However, neurons can also be classified by attributes such as axon laterality, axon projection range, connectivity, and neurotransmitter types (*4*–*6*). These classification axes often do not align with lineage-based axes, but rather their intersections generate the matrix from which neuronal diversification unfold. A prominent example is the binary division of all neurons into two groups: contralateral (commissural) and ipsilateral projection, based on whether their axons cross the midline or not. Each of the two groups is highly heterogenous comprising a mixture of neuron classes with distinct lineages. Conversely, many diverse neuron classes, defined developmentally by their lineages and distinct combinations of transcription factors (TFs), contain a mixture of commissural and ipsilateral neurons (*1*, *4*, *7*). To date, the genetic programs that instruct the partitioning of neurons based on their axon laterality are still poorly understood.

Commissural neurons play a critical role in connecting neuronal information between the two halves of the bilaterian nervous system. Despite their high heterogeneity, they all share the core defining feature of projecting their axons across the midline. The axon guidance mechanisms underlying this feature are fairly conserved and well understood (*8*, *9*). In vertebrates, most commissural neurons in the spinal cord, hindbrain, and midbrain project ventrally to cross the midline at the floor plate (FP) (*10*). Guidance of commissural axons toward the FP predominantly relies on signaling between the ligand Netrin-1, which is expressed from the FP and the ventral neural progenitors, and its receptor deleted in colorectal carcinoma (DCC) assisted by Robo3, both of which are expressed in commissural neurons (*8*, *9*, *11*, *12*). Another ligand-receptor pair, Shh and Boc, makes an additional but minor contribution to this process (*13*, *14*). Knockout (KO) mice of *Netrin-1*, *DCC*, or *Robo3* showed disrupted ventral commissure formation, among which *Robo3* KO mice showed a complete lack of ventral commissures in the spinal cord and hindbrain (*11*, *12*, *15*–*18*). Robo3 was proposed to silence the Slit-Robo1/2–mediated repulsion from the midline in pre-crossing commissural axons (*17*). A later study showed that mammalian Robo3 can interact with DCC and facilitate Netrin-1 signaling, hence directly promoting extension of commissural axons toward the midline (*19*). In addition, a third function of Robo3 is to mediate repulsive signal from its ligand NELL2 that helps keep commissural axons away from the motor column (*20*). Robo3 is transiently expressed in pre-crossing but is quickly down-regulated in post-crossing commissural axons/neurons (*11*, *17*), and mouse Robo3 is the only now known molecule that is exclusively expressed in FP-crossing commissural neurons from the spinal cord to the midbrain (*7*, *10*–*12*, *17*, *21*). DCC, however, shows more broad expression, including some ipsilaterally projecting neurons (*22*–*24*). Therefore, what determines the presence or absence of Robo3 in a neuron is likely to constitute the core of the genetic program that partitions neurons into commissural and ipsilateral categories.

There is limited knowledge on how *Robo3* transcription is regulated in commissural neurons. LIM-homeodomain (HD) TFs, LIM homeobox protein 2/9 (Lhx2/9), have been shown to control Robo3 expression in the commissural neurons of spinal dorsal interneuron class dI1 neurons, and Lhx2 appears to bind to the *Robo3* promoter (*25*). However, Lhx2/9 expression in developing mouse spinal cord is confined to dI1 class, leaving the Robo3 expression in other spinal classes yet to be accounted for. In the midbrain and the hindbrain preBötzinger complex, neural progenitors expressing the HD-TF Dbx1 give rise to commissural neurons. KO or knockdown of *Dbx1* affects contralateral axon projections, whereas forced expression of

[1]National Institute of Genetics, Graduate University for Advanced Studies, Sokendai, Yata 1111, Mishima, Shizuoka 411-8540, Japan. [2]Department of Medical Chemistry, Kansai Medical University, Hirakata, Osaka 573-1010, Japan. [3]Department of Medical Neurobiology, IMRIC, Hebrew University - Hadassah Medical School, Jerusalem, Israel.
*Corresponding author. Email: yanzhu@nig.ac.jp, yanzhu2007@gmail.com
†Present address: Division of Embryology, National Institute for Basic Biology, Higashiyama 5-1, Myodaiji, Okazaki 444-8787, Aichi, Japan.

Dbx1 in the midbrain induces ectopic Robo3 expression and contralateral axon projection (*21*, *26*). However, Dbx1 can only account for the part of commissural neurons that are derived from Dbx1-positive progenitors. These data raise the possibility that Robo3 might be separately regulated by different sets of TFs in distinct classes of commissural neurons. However, the fact that a highly conserved spatial and temporal distribution of Robo3 has been observed across divergent amniote species suggests that a conserved, possibly common, regulatory program is likely to operate (*10*).

In this study, we addressed the transcriptional mechanism that controls Robo3 expression. The components of an immediate upstream regulatory program of Robo3 are likely to be enriched in the pre- versus post-crossing commissural neurons, reflecting its temporal dynamics (*11*, *17*). On the basis of this assumption, we took advantage of the results from our RNA sequencing (RNA-seq) experiment that compared transcriptomes between pre- and post-crossing pontine nucleus (PN) neurons in murine hindbrains (to be published elsewhere) and identified an enrichment of a pair of closely related basic helix-loop-helix (bHLH) TFs, *Nhlh1* and *Nhlh2*, in the pre-crossing population. Nhlh1/2 (previously known as Nscl1/2 and Hen1/2) are expressed in immature neurons (*27*, *28*), but their roles in neural development have not been thoroughly explored, particularly in the context of a double deficiency of both genes (*29*–*31*). We found that forced expression of Nhlh1/2 could induce ectopic Robo3 expression, and *Nhlh1/2* and *Robo3* show correlated expression in the neural tube. By generating an *Nhlh1/2*-double-deficient mouse line, we were able to show that Nhlh1/2 comprise a global transcriptional mechanism that induces Robo3 expression in all FP-crossing commissural neurons from the spinal cord to the midbrain.

RESULTS

To separate relatively pure pre- and post-crossing commissural neurons is not trivial, as, during development, the pre- and the post-crossing as well as the commissural and ipsilateral-projecting neurons intermingle extensively. Therefore, we turned to a specialized group of commissural neurons, the precerebellar PN neurons in the hindbrain, whose cell bodies migrate tangentially over a considerable distance from the dorsal edge of the hindbrain to settle next to the ventral midline (*32*). The migration of PN neurons toward the midline requires Netrin-1/DCC/Robo3 signaling (*11*, *33*). While the leading processes of PN neurons cross the midline, their cell bodies mostly terminate migration without midline crossing. This developmental feature enables considerable spatial separation of two PN populations: those in the early- and mid-migratory routes harboring the pre-crossing and those near the midline region harboring the post-crossing leading processes. We took advantage of this feature to obtain pure populations of pre- and post-crossing PN neurons and compared their transcriptomic profiles (to be published elsewhere). We found that a pair of highly related class II bHLH TFs, *Nhlh1* and *Nhlh2*, was highly enriched in the pre-crossing (during migration), but was markedly down-regulated in the post-crossing (at final destination), PN neurons (enrichment: 54.52-fold for *Nhlh1* and 9.88-fold for *Nhlh2*). This differential expression of *Nhlh1* and *Nhlh2* was confirmed by in situ hybridization (ISH) expression data from the Allen Developing Mouse Brain Atlas (https://developingmouse.brain-map.org/) (fig. S1, A and B).

Nhlh1 and Nhlh2 could induce Robo3 expression as transcriptional activators

The enrichment of *Nhlh1* and *Nhlh2* in pre-crossing PN neurons suggests that they might regulate the expression of genes required for the behavior of the pre-crossing PN neurons. Therefore, we screened for Nhlh1/2 binding sites in the promoter/enhancer regions of genes that were enriched in the pre-crossing PN population from our RNA-seq data using the position frequency matrices of Nhlh1 and Nhlh2 from JASPAR (http://jaspar.genereg.net) (*34*). The screen singled out *Robo3*, a gene known to be highly expressed in migrating PN neurons (*11*). Using UCSC genome browser (http://genome.ucsc.edu) (*35*) and its built-in tools, we identified a potential Nhlh1/2 binding site in the *Robo3* proximal promoter (GRCm38/mm10, chr9:37,433,247-37,433,566) and four Nhlh1/2 binding sites in a distal region 26-kb 5′ to the *Robo3* transcription start site (GRCm38/mm10, chr9:37,459,714-37,461,104) (fig. S1C). This distal region, which we named as *eR3-Nhlh*, contains four subregions that show hallmarks of an enhancer element, and the sequences encompassing the four Nhlh1/2 binding sites are conserved across mammals, suggesting that they might be important for regulating *Robo3* expression. The in silico analysis of *Robo3* cis-regulatory region raised the possibility that Nhlh1 and Nhlh2 might regulate *Robo3* transcription.

To test this possibility, we asked whether forced expression of Nhlh1 and Nhlh2 could induce ectopic Robo3 expression. We introduced expression vectors of full-length (fl) *Nhlh1* and *Nhlh2* into the lower rhombic lip of mouse hindbrains, or the midbrains, via in utero electroporation (EP) at embryonic day 12.5 (E12.5) and analyzed Robo3 protein expression at E14.5 (Fig. 1, A to C). The lower rhombic lip region situated at the dorsal edge of the caudal hindbrain (Fig. 1B, schematic) contains the progenitor zone of PN neurons (*36*, *37*) but is devoid of Robo3 expression (Fig. 1, B and E) because postmitotic PN neurons only express Robo3 after leaving the rhombic lip. Forced expression of Nhlh1/2 in the rhombic lip clearly induced the ectopic expression of Robo3 within the rhombic lip region (Fig. 1B and fig. S2A). Electroporated neurons found deep within the hindbrain neuroepithelium also expressed ectopic Robo3 (Fig. 1B). In the midbrain at E14.5, endogenous Robo3 is barely detectable, but the electroporated site clearly showed ectopic Robo3 expression (Fig. 1C and fig. S2A). *Robo3* ISH on electroporated samples indicated that the ectopic expression of *Robo3* was induced at a transcriptional level (fig. S2B). EP of *Nhlh1* or *Nhlh2* alone also induced ectopic Robo3 expression (fig. S2, C and D). In contrast, EP of full-length *Lhx2*, a molecule previously shown to directly control *Robo3* transcription in dI1 spinal neurons (*25*, *38*), did not induce ectopic Robo3 expression in the rhombic lip and the midbrain (fig. S2E). These results showed that force-expressing Nhlh1 and Nhlh2 induced ectopic *Robo3* transcription.

Next, we asked how Nhlh1/2 induce Robo3 expression and which of their domains are important for Robo3 induction. Nhlh1 and Nhlh2 share a highly homologous canonical bHLH domain in the C terminus and a poorly conserved low-complexity domain in the N terminus (Fig. 1D) (*39*, *40*). Immediately preceding the canonical bHLH domain, both molecules contain a highly conserved stretch of 11 amino acids, encompassing six or five consecutive arginine (R) residues. This stretch, which we named the R6 domain, is a feature specific to Nhlh1/2 (*40*). The highly charged R6 domain was speculated to form a part of an extended basic domain together with the canonical basic region, rendering the DNA binding specificity

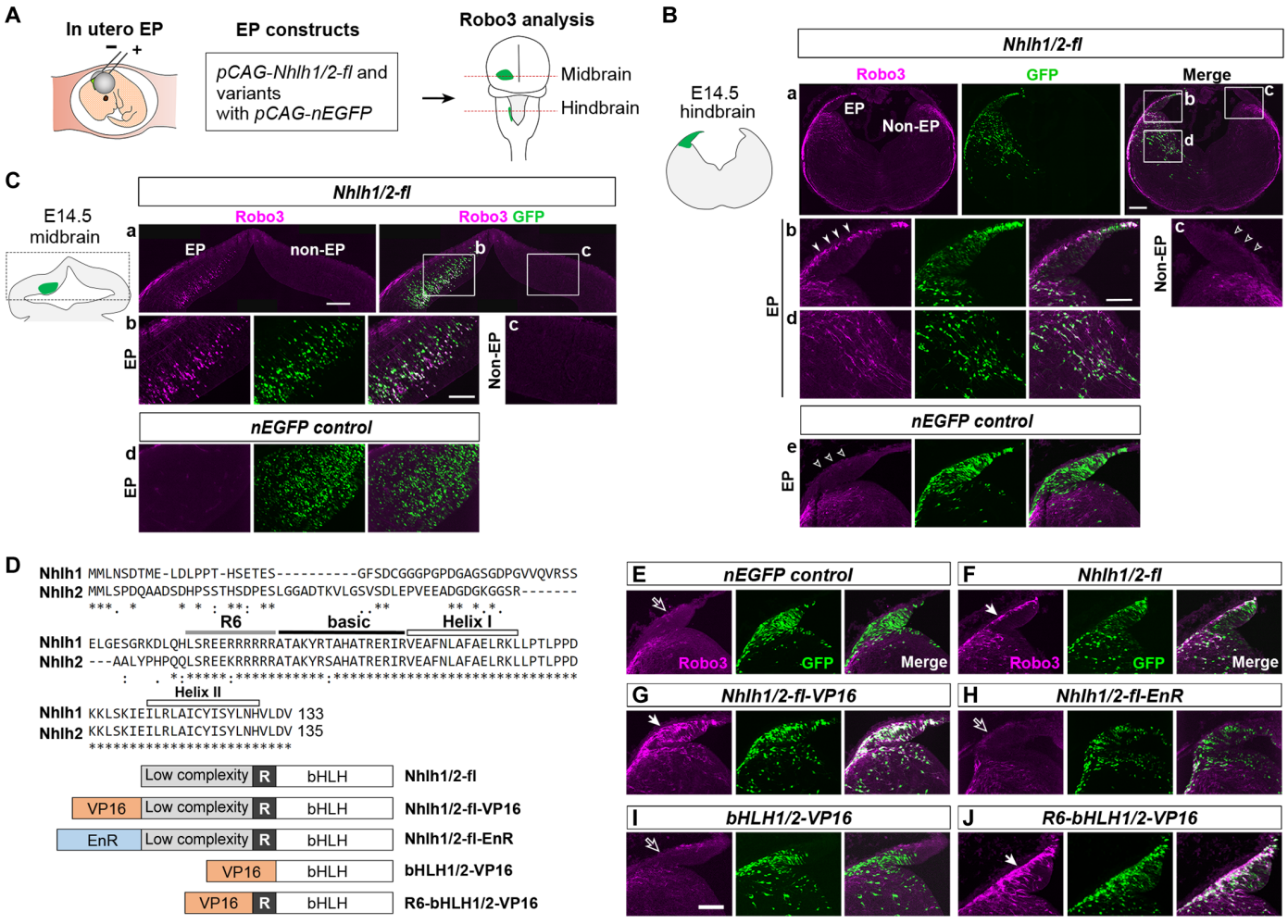

Fig. 1. Nhlh1 and Nhlh2 forced expression induce ectopic Robo3 expression in mouse hindbrain and midbrain, as transcriptional activators. (**A**) Experimental procedure schematic. Embryos were electroporated at embryonic day 12.5 (E12.5) and analyzed at E14.5. (**B**) EP of full-length *Nhlh1* and *Nhlh2* into the dorsal hindbrain including the rhombic lip region (green in the schematic). EP and non-EP stand for electroporated and non-electroporated sides, respectively. (Ba) A low-magnification image of a section with Robo3 and GFP immunohistochemistry (IHC). [(Bb) to (Bd)] High-magnification images of (b), (c), and (d) boxes in (Ba). The EP side [filled arrowheads in (Bb)], but not the non-EP side [hollow arrowheads in (Bc)], showed induction of ectopic Robo3 expression ($n = 6$). (Bd) Ectopic Robo3 induction deep in the hindbrain epithelium. (Be) EP of *nEGFP* alone did not induce Robo3 in the rhombic lip. (**C**) EP of full-length *Nhlh1* and *Nhlh2* unilaterally into the dorsal midbrain region (green in the schematic). (Ca) The EP, but not the non-EP side, showed ectopic Robo3 induction ($n = 6$). [(Cb) and (Cc)] High-magnification images of (b) and (c) boxes in (Ca). (Cd) EP of *nEGFP* alone did not induce Robo3 in the midbrain. (**D**) Top: Sequence alignment of Nhlh1 and Nhlh2 proteins and their domain structures. Bottom: Variants of Nhlh1/2 being tested for Robo3 induction. (**E** to **J**) The rhombic lip regions electroporated with the DNA constructs indicated above. Filled arrows indicate ectopic Robo3 induction in the rhombic lip in [(F), $n = 6$], [(G), $n = 3$], and [(J), $n = 3$]. Hollow arrows indicate lack of Robo3 induction in [(E), $n = 5$], [(H), $n = 3$], and [(I), $n = 3$]. Scale bars, 200 μm (Ba), 100 μm [(Bb) to (Be)], 200 μm (Ca), 100 μm [(Cb) to (Cd)], and 100 μm [(E) to (J)].

unique to Nhlh1/2 (*41*). Evidence exists on both sides for the role of Nhlh1/2 as activators or repressors (*30*, *42*–*44*). To distinguish these possibilities, we generated two types of Nhlh1/2 fusion molecules: (i) fusion with a potent trans-activating domain from the herpes simplex virus TF VP16 (*45*); and (ii) fusion with a potent repressor domain, EnR, from the Drosophila Engrailed (*46*) (Fig. 1D). We electroporated the fusion constructs into E12.5 brainstems as above and assayed for Robo3 induction in the rhombic lip and the midbrain. The successful expression of these *VP16*- and *EnR*-fusion *Nhlh1/2* variants in the rhombic lip and the midbrain were confirmed by *VP16* and *EnR* ISH (fig. S2J). VP16-fused Nhlh1/2-fl, like Nhlh1/2-fl, induced high level of Robo3 expression in the rhombic lip (Fig. 1, G and F, compare to Fig. 1E). It also induced strong Robo3 expression in the midbrain (fig. S2F). In contrast, EnR-fused Nhlh1/2-fl failed to induce ectopic Robo3 expression in the rhombic lip (Fig. 1H) and the midbrain (fig. S2G), although they were properly targeted into nuclei (fig. S2K). These results suggest that Nhlh1/2 serve as transcriptional activators to induce Robo3 expression. We then investigated the functional importance of the R6 domain in Robo3 induction. VP16 fused directly to the canonical bHLH domain without the R6 domain and the N-terminal half did not induce Robo3 expression despite their being properly targeted into nuclei (Fig. 1I and fig. S2, H and K). By contrast, adding only the R6 domain to the above construct turned the fusion protein into a potent inducer of Robo3 (Fig. 1J and fig. S2I). These results indicate that the R6 domain unique to the Nhlh1/2 subfamily, together

with the canonical bHLH domain, is essential for Nhlh1/2 to activate Robo3 expression.

Forced expression of Nhlh1 and Nhlh2 drives contralateral axon projections

The observation that Robo3 was induced by Nhlh1/2 prompted us to ask whether forced expression of Nhlh1/2 could instruct axon projections toward the ventral midline and hence rendering commissural neuronal identity. To address this, we force-expressed Nhlh1/2 in the developing midbrain and hindbrain as in Fig. 1 and examined the axon trajectories of the electroporated neurons. In the midbrain, we used a previously established method that enabled the examination of axon laterality in flat-mounted brainstem after in utero EP (Fig. 2A) (*21*). EP with an *mCherry* expression construct into the midbrain at E11.5 labeled almost entirely caudally extending ipsilateral axons examined at E14.5 with only 6.4% (± 3.8%) of all labeled axons projecting contralaterally, in line with the previous report (Fig. 2, B and C) (*21*). Forced expression of Nhlh1/2 at E11.5 directed 23% (± 7.6%) of all labeled axons to project contralaterally (Fig. 2, B and C). In the hindbrain, control EP with an *EGFP* construct at E12.5 should label a mixture of ipsilateral-projecting and commissural neurons, with the latter comprising mainly PN neurons that migrate anteriorly for some distance before turning toward midline. Therefore, in sections from caudal hindbrain, we found only a few neurons whose axons extend ventrally toward midline at E14.5, resulting in low levels of green fluorescent protein (GFP)

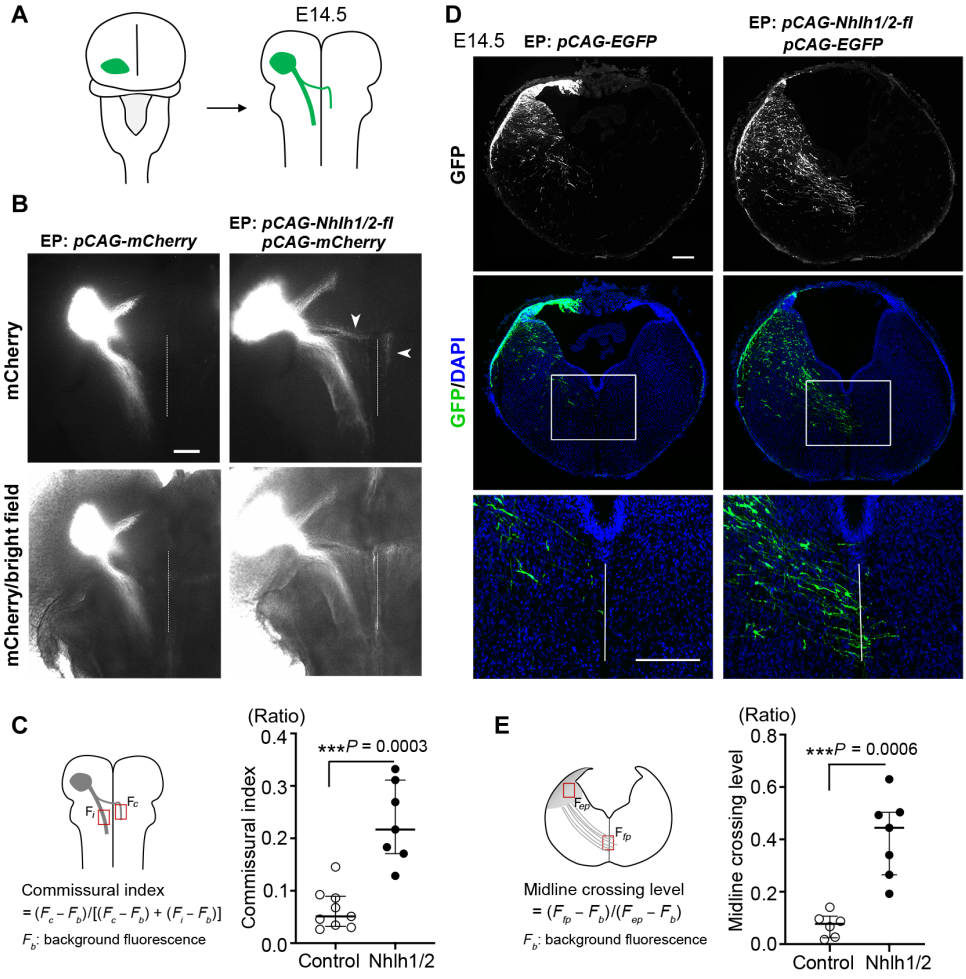

Fig. 2. Forced expression of Nhlh1 and Nhlh2 drives axonal projection toward the ventral midline. (**A**) A schematic showing the procedure of assaying the laterality of the labeled midbrain axons. EP was performed at E11.5 and the labeled midbrain axon tracts analyzed on flat-mounted brainstems at E14.5. (**B**) Partial views of samples electroporated with either *mCherry* ($n = 9$) or with *Nhlh1/2* and *mCherry* constructs ($n = 7$). Top: Fluorescence images. Bottom: Merged fluorescence and bright-field images to visualize the tissue outlines and the ventral midlines (white vertical lines). (**C**) Quantification of the midbrain EP experiment. The schematic on the left shows how the commissural index was quantified (see Materials and Methods). The data were represented by a scatter plot with the median and the upper and lower quantiles indicated. Force-expressing Nhlh1 and Nhlh2 markedly increased the proportion of axons that crossed the ventral midline ($P = 0.0003$, Mann-Whitney *U* test). (**D**) The effect of expressing *Nhlh1/2* and *EGFP* ($n = 6$) in comparison to expressing only *EGFP* ($n = 7$) on hindbrain axons. EP was performed at E12.5, and samples were analyzed at E14.5 after green fluorescent protein (GFP) IHC. Bottom: High-magnification images around the ventral midline (white vertical lines) corresponding to the boxes in the middle panel. (**E**) Quantification of the hindbrain EP experiment. The schematic on the left shows how the midline crossing level was quantified (see Materials and Methods). The data were represented by a scatter plot with the median and the upper and lower quantiles indicated. Force-expressing Nhlh1 and Nhlh2 markedly increased the proportion of axons and neurons that reached the ventral midline ($P = 0.0006$, Mann-Whitney *U* test). Scale bars, 400 μm (B) and 200 μm (D).

fluorescence at the midline region (Fig. 2, D and E). In contrast, EP of *Nhlh1*/2 increased the number of *GFP*-labeled neurons that either extended their axons or migrated toward the midline, resulting in significantly higher GFP signals than that of the control (Fig. 2, D and E). Together, these results show that forced expression of Nhlh1/2 could drive changes in axonal projection from ipsilateral to contralateral, suggesting that axon laterality in vivo might be determined by the presence or absence of a pair of TFs.

Comparison of the expression of *Nhlh1* and *Nhlh2* in relation to *Robo3* during the development of commissural neurons

If Nhlh1/2 positively regulate Robo3 expression in vivo, we would expect them to be expressed in Robo3 expressing commissural neurons. Robo3 has previously been shown to be expressed and required in all commissural neurons whose axons cross the ventral midline at the FP, which spans from the spinal cord to the midbrain (*10*–*12*, *17*, *21*). In the forebrain, the FP ceases to exist (*47*), and Robo3 expression is absent from the forebrain commissural tracts (*10*). We examined the expression patterns of *Nhlh1* and *Nhlh2* in relation to that of *Robo3* at stages when FP-crossing commissural axon projections take place.

Due to the lack of good antibodies for Nhlh1 and Nhlh2, we turned to ISH using *Nhlh1*, *Nhlh2*, and *Robo3* riboprobes on adjacent sections. *Nhlh1*, *Nhlh2*, and *Robo3* expression was first examined in migrating PN neurons at E14.5. Consistent with our RNA-seq and the ISH expression data from the Allen Developing Mouse Brain Atlas (fig. S1), we found that both *Nhlh1* and *Nhlh2* were expressed in migrating PN neurons, similar to *Robo3* expression (Fig. 3A). Next, we examined the expression of these three molecules across the entire neuroaxis of the central nervous system (CNS) at E11.5 when most commissural neurons are specified and send their axons toward the FP. *Robo3* was generally expressed in immature neurons immediately adjacent to the ventricular zone but not in more differentiated neurons at superficial positions (Fig. 3, B to E), consistent with previous findings (*11*, *17*). The expression pattern of *Nhlh1* and *Nhlh2* within the CNS was also mostly confined to immature neurons adjacent to the ventricular zone, and the combined expression regions of *Nhlh1* and *Nhlh2* appeared to include all the *Robo3* expression regions (Fig. 3, B to E). We also examined their expression in the spinal cord at E10.5, an early stage of commissural neuron development, and found that *Nhlh1* and *Nhlh2* were already expressed in the *Robo3*-positive region (Fig. 3B). Two points worth noting here. First, combined expression of *Nhlh1* and *Nhlh2* appeared wider than that of *Robo3*. For example, *Nhlh1*/2 are expressed in the ventral spinal cord including what appears to be the motor neuron (MN) domain that is devoid of *Robo3* expression (Fig. 3B).

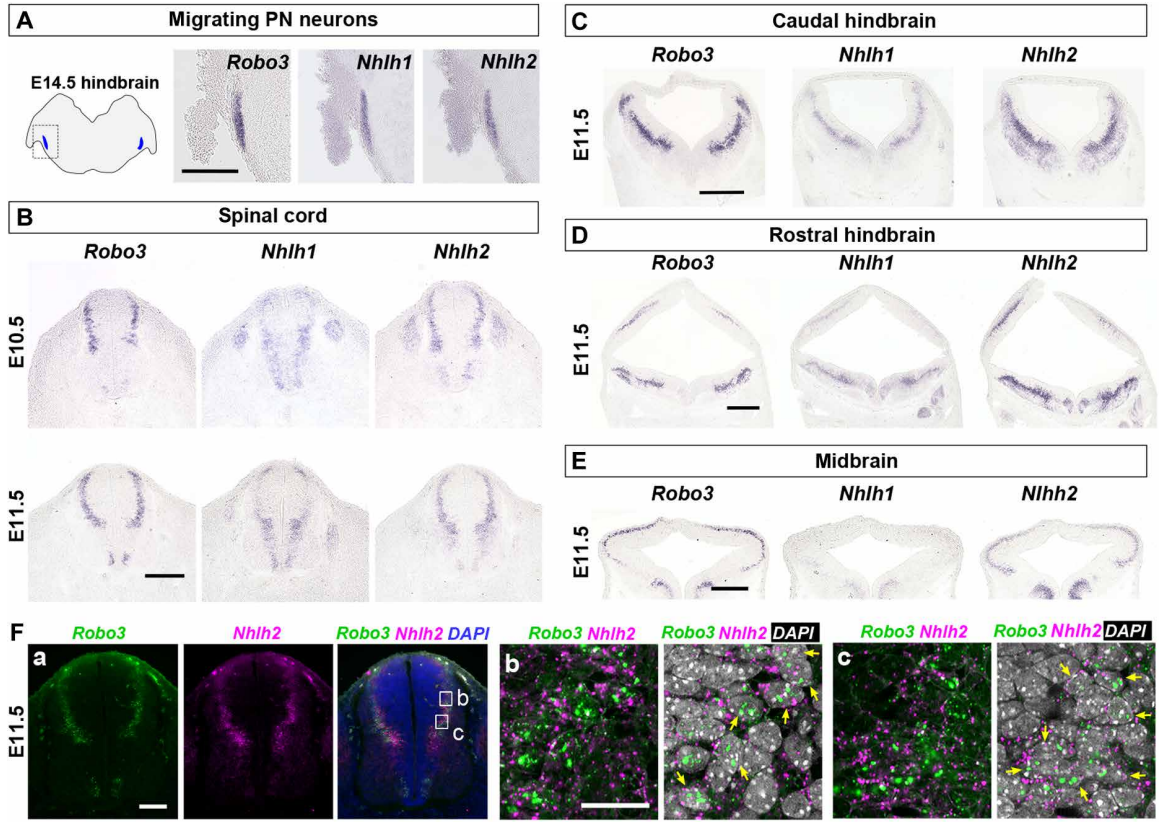

Fig. 3. Expression of *Robo3*, *Nhlh1*, and *Nhlh2* on adjacent sections from the spinal cord to the midbrain shown by ISH. (**A**) The schematic on the left shows a hindbrain section at E14.5 with the cross sections of migrating PN neurons in blue. The boxed area corresponds to the region of the ISH images on the right. (**B**) E10.5 (top) and E11.5 (bottom) spinal cord sections. (**C**) Caudal hindbrain sections at E11.5. (**D**) Rostral hindbrain sections at E11.5. (**E**) Midbrain sections at E11.5. (**F**) Double-fluorescence ISH of *Robo3* and *Nhlh2* on an E11.5 spinal cord section. (Fa) Low-magnification images showing the overall *Robo3* and *Nhlh2* signals resembling the colorimetric ISH signals in (B). [(Fb) and (Fc)] High-magnification single focal plane confocal images of the box areas (b) and (c) in (Fa). Yellow arrows indicate neurons containing both *Robo3* and *Nhlh2* RNA particles within the same cell. Scale bars, 200 μm [(A), (B), and (E)], 400 μm [(C) and (D)]; 100 μm (Fa), and 25 μm [(Fb) and (Fc)].

The expression of *Nhlh1* in the early MNs has been reported in a previous study (*27*). Second, the *Nhlh1* and *Nhlh2* expression domains mostly overlap, although the relative expression level between *Nhlh1* and *Nhlh2* appeared to vary depending on brain regions and neuronal subdomains. For example, *Nhlh1* expression was stronger than *Nhlh2* in the ventral-most spinal domain, whereas *Nhlh2* was stronger in the dorsal spinal cord (Fig. 3B). In the E11.5 midbrain, the *Nhlh1* signal was very weak yet still detectable as a faint band of signal correlating to the *Robo3* pattern. In brain regions rostral to the midbrain, the expression of *Robo3*, *Nhlh1*, and *Nhlh2* was no longer well correlated (fig. S3, A to C).

To demonstrate co-expression of *Nhlh1/2* and *Robo3* at a single-cell level, we then performed double-fluorescence ISH using *Nhlh2* and *Robo3* riboprobes on E11.5 spinal cord sections. Most cells that contain *Robo3* RNA particles were found to also contain *Nhlh2* RNA particles within the bounds of the same cells (Fig. 3F, 90.2 ± 3.1% of 133 Robo3$^+$ cells, eight image fields from three sections). This result, together with the overall expression patterns, raises the possibility that Nhlh1/2 might regulate Robo3 expression broadly across a large part of the neural tube.

All FP-crossing commissural axons from the spinal cord to the midbrain fail to approach the ventral midline in *Nhlh1*- and *Nhlh2*-double-deficient mice

To examine the endogenous function of Nhlh1 and Nhlh2, we generated *Nhlh1*- and *Nhlh2*-deficient mice by CRISPR-Cas9–mediated gene editing in germ line cells (fig. S4, A and B). The resultant *Nhlh1* mutant allele (*Nhlh1-m*) carries a premature termination codon just before the first helix region, thus generating a truncated Nhlh1 protein without the HLH region (fig. S4C). The *Nhlh2-m* allele carries corrupted amino acids over the extended basic domain and the first helix regions (fig. S4D), resulting in a peptide that could no longer generate the bHLH structure. Given that the bHLH region is essential for DNA binding and protein-protein interactions of bHLH TFs (*48*), we expect that *Nhlh1-m* and *Nhlh2-m* are loss-of-function alleles. To confirm this, we cloned the coding sequences of *Nhlh1-m* and *Nhlh2-m* into expression vectors and found that forced expression of Nhlh1-m and Nhlh2-m in E12.5 mouse embryos by EP did not induce an ectopic expression of Robo3 in the rhombic lip or in the midbrain (fig. S4, E, F, and H). We also confirmed that Nhlh1-m and Nhlh2-m did not act dominant negatively in suppressing Robo3 expression, because PN neurons expressing Nhlh1-m and Nhlh2-m showed normal Robo3 expression (fig. S4, G and H).

We then generated single and double homozygotes of *Nhlh1-m* and *Nhlh2-m*. Targeted KO of *Nhlh1* and *Nhlh2* has been previously generated (*29*, *49*, *50*), and, in addition to perinatal lethality, only two defects in the developing brain have been reported in the double KO (dKO) mice: defects in the migration of PN neurons (*31*) and gonadotropin-releasing hormone (GnRH)–expressing neurons (*30*). However, the mechanisms underlying these defects have not been elucidated. We first analyzed PN formation in the double *Nhlh1/2* mutant. We found that PN neurons failed to migrate toward the ventral midline but instead arrested migration in the lateral and anteriorly extended positions (Fig. 4A). This phenotype highly resembled what was previously reported in dKO mice (*31*). PN formation in single *Nhlh1* and *Nhlh2* mutants appeared normal, also in line with the previous report (fig. S5A) (*31*). The PN phenotypes observed in the present study, as well as in the previous dKO, are highly reminiscent of the PN defect in the *Robo3* mutant (*11*). Another precerebellar nucleus, the inferior olivary nucleus (ION), is also affected in the *Robo3* mutant (*11*). We found that, in the double mutant of *Nhlh1/2*, ION neurons failed to gather tightly around the ventral midline as in the control but were situated at a small distance away from the midline, a phenotype that again resembled that of the *Robo3* mutant (fig. S5, B and C).

We next examined ventral commissure formation along the neuroaxis from the spinal cord to the midbrain in our mutant mice. Tag1 (also known as Contactin2) was used as a marker for commissural axons (*51*), and neurofilament (NF) was used to reveal the overall axonal patterns. We found that ventral commissures completely failed to form in the double mutant in the spinal cord (Fig. 4B), the hindbrain (Fig. 4C), and the midbrain (Fig. 4D). The NF staining showed rigorous axon extensions, suggesting that the double mutant does not affect the ability of neurons to extend axons (Fig. 4, B to D). Tag1-positive axons initially developed similarly between the control and the double mutant in the dorsal neural tube, but they appeared to fail to converge and extend all the way to the ventral midline in the latter. No notable abnormalities in the ventral commissure formation were observed in the single mutants of *Nhlh1* and *Nhlh2* (fig. S5, D to G). The prevalent absence of ventral commissures persisted into later stages, as shown by analyses of the E13.5 and E16.5 spinal cord (fig. S5, H and I) and the E13.5 hindbrain and midbrain (fig. S5, J and K).

The non-FP crossing commissures, such as dorsally crossing commissural axons or commissures anterior to the midbrain, develop independently of Robo3 (*4*, *10*, *52*). We found that the dorsal commissure in the spinal cord, anterior commissure in the basal forebrain, and corpus callosum were all normal in the double mutant (fig. S6, A to C). This result indicates that Nhlh1/2 deficiency specifically affects commissural axons that cross the FP.

A large reduction of Robo3 in *Nhlh1* and *Nhlh2* double mutant

The FP-crossing commissures failed to form in the *Nhlh1/2* double mutant, resembling the defects observed in the *Robo3* mutant. We next investigated Robo3 expression in the *Nhlh1/2* double mutant by Robo3 immunohistochemistry (IHC). We found that Robo3 expression was barely detectable in the E11.5 spinal cord (Fig. 5A), the hindbrain (Fig. 5B), and the midbrain (Fig. 5C) of the double mutant. Similarly, a large reduction in Robo3 was also observed in the migrating PN neurons at E16.5 (Fig. 5D). Examination of *Robo3* transcription by ISH also revealed a marked reduction in *Robo3* mRNA in the spinal cord (Fig. 5E) and the migrating PN neurons (Fig. 5F) in the double mutant. These results provide the compelling evidence that Nhlh1/2 are responsible for Robo3 expression in vivo.

Two lines of evidence suggest that Robo3 deficiency is the primary cause of the commissure phenotype observed in the *Nhlh1/2* double mutant. First and foremost, the Robo3 expression level was barely detectable in the *Nhlh1/2* double mutant, whereas the expression of *Netrin-1* and *Shh*, the two guidance molecules responsible for guiding commissural axons toward the midline (*14*, *16*), and the Netrin-1 receptor DCC was readily detectable in the double mutant (fig. S7, A to C). Accordingly, the commissure phenotype in *Nhlh1/2* double mutant closely resembles that of the *Robo3* mutant (*11*, *12*, *17*) but not that of mice deficient in Netrin-1 or Shh signaling (*8*, *9*, *13*–*16*, *19*, *33*). For example, a small number of commissural axons remained intact in the *Netrin-1* or *DCC* mutant, and some affected commissural axons invaded into the ventricular zone. These phenotypic features were not

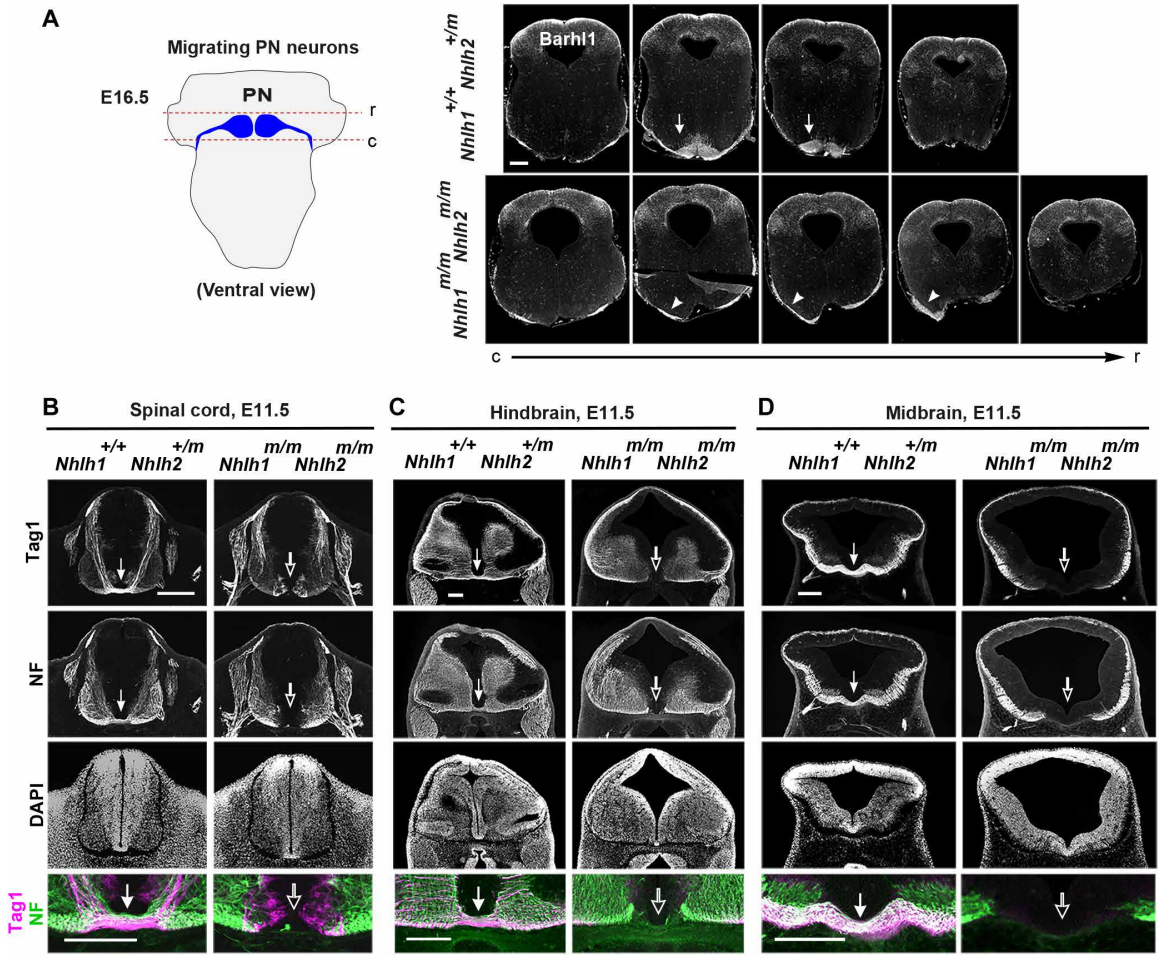

Fig. 4. Lateralized PN and a complete lack of ventral commissures in the spinal cord, hindbrain, and midbrain in *Nhlh1* and *Nhlh2* double mutant. (**A**) The schematic shows the PN formation in an E16.5 hindbrain. Red dashed lines mark the rostral (r) and caudal (c) span of the sections shown on the right. PN is visualized by Barhl1 IHC. PN neurons form a nucleus adjacent to the ventral midline (arrows) ($n = 3$) in the control but were laterally positioned (arrowheads) indicating failure to approach the ventral midline in the mutants ($n = 3$). (**B** to **D**) Coronal sections from the spinal cord (B), hindbrain (C), and midbrain (D) at E11.5 were subjected to Tag1 and NF double IHC with the Tag1 labeling the commissural axons and the NF signals depicting the general axonal patterns. The DAPI counterstain indicates the overall cytoarchitecture. Comparisons were made between the control genotype ($Nhlh1^{+/+}$ $Nhlh2^{+/m}$) ($n = 3$) and the double mutant ($Nhlh1^{m/m}$ $Nhlh2^{m/m}$) ($n = 3$). The Tag1 and NF merged images in the bottom panel are high-magnification images of the ventral commissure regions. The double mutant showed a complete lack of ventral commissures (hollow arrows), in comparison to the control (filled arrows). Scale bars, 200 μm [(A) to (D)].

observed in the *Robo3* and *Nhlh1/2* mutants. Second, the initial fate specification and axon extension did not appear to be affected in the double mutant. In the spinal cord, $Brn3a^{+}$ neurons comprising dI1, dI2, dI3, dI5, and the late born dILB dorsal spinal classes and the Lhx1-expressing dI2 and dI4 spinal classes (*3*, *7*), both containing a mixture of commissural and ipsilateral neurons, were comparable in number between the double mutant and the control (fig. S7, D and E). Tag1 and DCC, both being predominantly expressed in commissural neurons, showed normal initial axon extension in the dorsal half of the spinal cord in the double mutant (Fig. 4B and fig. S7C). In addition, the specification of the PN neurons also appeared to be normal in the double mutant, as these neurons migrated anteriorly and expressed the PN neuronal markers Barhl1 and DCC (Fig. 5D and fig. S7F).

Robo3 in regions rostral to the midbrain, where its expression was not correlated with that of *Nhlh1* and *Nhlh2* (fig. S3), was not downregulated in the double mutant. In the three forebrain structures known to express Robo3: the ganglionic eminence, hypothalamus, and medial habenular nucleus (mHb) (fig. S3) (*53*, *54*), we found that Robo3 expression was not affected (fig. S8, A to C). Axons from the mHb form a highly fasciculated tract fasciculus retroflexus (FR) that projects caudally through the midbrain and crosses the ventral midline at the midbrain/hindbrain junction (*54*). We found that the FR in the double mutant continued to express Robo3 (fig. S8D) and was able to approach and cross the ventral midline (fig. S8E), supporting our earlier conclusion that the extrinsic guidance program for midline crossing is intact in the double mutant. These results suggest that Robo3 expression in the forebrain is regulated by transcriptional program other than Nhlh1/2.

A conserved role of Nhlh1 and Nhlh2 in Robo3 induction in chick

FP, as a specialized ventral midline structure in developing neural tube, is conserved across the vertebrates (*47*). Robo3 exists in all vertebrates, and the spatial and temporal patterns of Robo3 expression

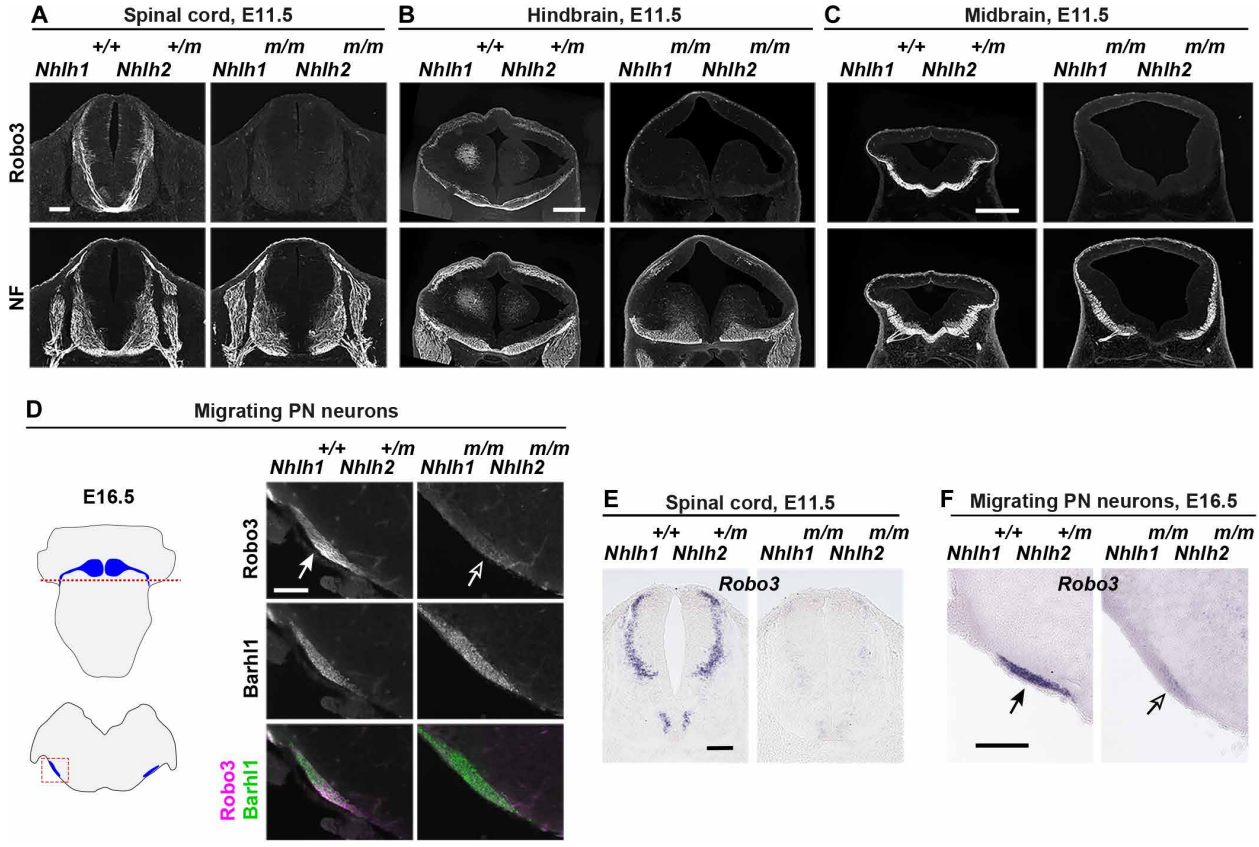

Fig. 5. A large reduction of Robo3 expression in commissural neurons in *Nhlh1* and *Nhlh2* double mutant. Coronal sections from the spinal cord (**A**), hindbrain (**B**), and midbrain (**C**) at E11.5 were subjected to Robo3 and NF double IHC. Robo3 expression level showed a marked reduction to almost the background level in the double mutant ($n = 3$) in comparison with the control ($n = 3$) at all axial levels from the spinal cord to the midbrain. (**D**) The schematics show the migrating PN neurons in a whole-mount E16.5 hindbrain in the top and on a coronal section in the bottom. The red dashed line and the boxed area indicate the approximate axial level and the area of IHC images on the right. PN neurons were labeled by Barhl1 IHC. A large reduction of Robo3 expression was detected in the PN neurons in the double mutant (hollow arrow) ($n = 3$) in comparison with the control (filled arrow) ($n = 3$). (**E** and **F**) *Robo3* ISH on E11.5 spinal cord and E16.5 hindbrain sections, respectively, showed a large reduction of *Robo3* mRNA in the double mutant. Scale bars, 100 μm [(A), (D), and (E)], 400 μm [(B) and (C)], and 200 μm (F).

in diverse amniotes species showed a high degree of conservation suggesting its regulation by conserved genetic program (*10*). Could Nhlh1/2 be an evolutionarily conserved genetic program in regulating Robo3? Orthologs of Nhlh1 and Nhlh2 were only found in the vertebrates. In the phylogenetic tree of Nhlh1 and Nhlh2 across vertebrate lineages (Fig. 6A), Nhlh2 is present across vertebrate species, whereas Nhlh1 appears missing in cartilaginous and ray-finned fishes. To test whether Nhlh1/2 may have a conserved function in vertebrates, we turned to chick spinal cord. We first examined the expression patterns of *Nhlh1* and *Nhlh2* in relation to *Robo3* in the developing chick spinal cord. The expression of *Robo3* in chick resembled that in mice (Fig. 6B compare to Fig. 3B), in agreement with previous studies (*55*). The expression patterns of chick *Nhlh1* and *Nhlh2* in the spinal cord were also highly reminiscent of those in mice (Fig. 6B), in that both genes were expressed in immature neurons adjacent to the ventricular zone and their combined expression region included the Robo3 expression region. We next examined whether in ovo EP of mouse *Nhlh1*/2 into chick spinal cord could induce chick Robo3 expression. We detected Robo3 induction on the EP side of the spinal cord by both IHC and ISH (Fig. 6C). Notably, ectopic expression of Nhlh1/2 induced broad Robo3 expression even in the ventral half of the spinal cord (Fig. 6C, arrow), which contains the ipsilateral projecting V1, V2, and MN spinal neurons. These results suggest that the role of Nhlh1/2 in Robo3 induction might be conserved in chick and, therefore, raises the possibility that using Nhlh1/2 for Robo3 induction in FP-crossing commissural neurons might have emerged during early vertebrate evolution.

Nhlh1/2 activate transcription via their binding sites identified in a distal enhancer of *Robo3*

To test whether Nhlh1/2 transactivate *Robo3* expression directly via binding to Nhlh1/2 binding sites that we identified in silico (fig. S1C) in the genomic locus of *Robo3*, we took two approaches: chromatin immunoprecipitation combined with real-time quantitative polymerase chain reaction assay (ChIP-qPCR), and in vivo reporter assay in chick and mouse. For ChIP, we used mouse midbrain tissues electroporated with *HA*-tagged *Nhlh1/2-fl* and *nEGFP* for chromatin preparation and an anti-hemagglutinin (HA) antibody for immunoprecipitation. Four genomic regions were tested: *eR3-Nhlh-r1* and *eR3-Nhlh-r2* are located within the *Robo3* distal enhancer *eR3-Nhlh* and contain Nhlh1/2 binding sites; *DCC-2660* and *Robo3-7979* are located in the upstream regions of *DCC* and *Robo3* genes,

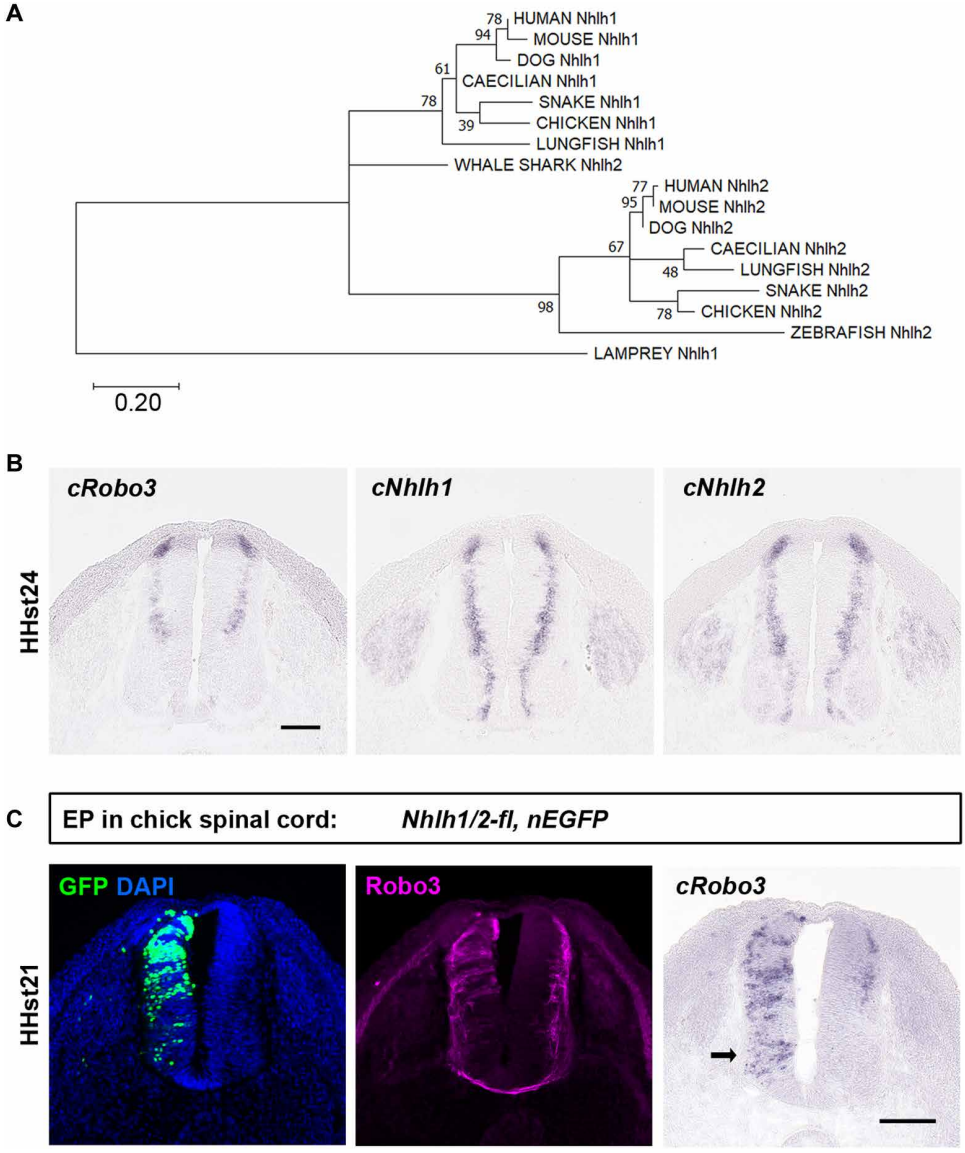

Fig. 6. The role of Nhlh1 and Nhlh2 in Robo3 induction is conserved in chick. (**A**) Nhlh1 and Nhlh2 orthologs are present throughout vertebrate lineages including birds, but not in invertebrates. The phylogenetic tree is rooted to Lamprey Nhlh1. Bootstrap support values are indicated at the branch points. Scale bar, substitutions per site. (**B**) ISH of chick (c) *Robo3*, *cNhlh1*, and *cNhlh2* on adjacent coronal sections of HHst24 chick spinal cord. (**C**) Full-length mouse *Nhlh1* and *Nhlh2* were force-expressed unilaterally in chick embryonic spinal cords by in ovo EP at HHst16/17. Induction of Robo3 was examined by IHC ($n = 11$) and ISH ($n = 6$) on adjacent coronal sections of EP samples at HHst21/22. Ectopic induction of Robo3 was readily detected on the EP side, pointing to a conserved role of Nhlh1 and Nhlh2 in Robo3 induction in chick. Scale bars, 100 μm [(B) and (C)].

respectively, and are devoid of Nhlh1/2 binding sites (figs. S1C and S9A). qPCR of these four genomic regions showed an enrichment of *eR3-Nhlh-r1* and *eR3-Nhlh-r2* in the HA antibody versus control IgG immunoprecipitated chromatin (fig. S9A). By contrast, the two genomic regions devoid of Nhlh1/2 binding sites showed negligible level of enrichment (fig. S9A). The ChIP-qPCR assay result demonstrates that Nhlh1/2 bind to the *Robo3* enhancer element, *eR3-Nhlh*, which contains a cluster of Nhlh1/2 binding sites.

We next tested the *eR3-Nhlh* enhancer activity and its dependency on the integrity of Nhlh1/2 binding sites using in vivo reporter assays in chick and mouse. Three reporter constructs were made comprising an *EGFP* gene driven by the *eR3-Nhlh* enhancer or its variations and the proximal promoter and 5′ untranslated region (5′UTR) of *Robo3* (fig. S9B). *eR3-Nhlh::EGFP* contains the wild-type upstream sequences, whereas *eR3-Nhlh*::EGFP* has a few Guanine Cytosine (GC)-rich stretches being changed to adenine thymine for the ease of synthesis of this region by gBlocks gene fragments (Integrated DNA Technologies). Using *eR3-Nhlh*::EGFP* as a template, mutations were introduced into the core E-Box sequences of the four Nhlh1/2 binding sites in *eR3-Nhlh*, resulting in a third construct *mut-eR3-Nhlh*::EGFP* (fig. S9B). Upon EP into the chick spinal cord, *eR3-Nhlh::EGFP* or *eR3-Nhlh*::EGFP* yielded expression of the reporter gene in commissural axons (fig. S9, C and D). For the *CAG::mCherry* and *eR3-Nhlh*::EGFP* co-EP samples, we

showed that, whereas *mCherry* gene driven by a ubiquitous promoter labels a mixture of ipsilateral-projecting and commissural axons (65 ± 11.08% commissural axons; fig. S9, D and E, magenta arrows), *eR3-Nhlh*::EGFP* predominantly labels the commissural axons (97 ± 2.44% commissural axons; fig. S9, D and E, green arrow). To test the requirement of the Nhlh1/2 binding sites in the reporter construct for the expression in commissural neurons, *mut-eR3-Nhlh*::EGFP* was co-electroporated with *CAG::mCherry*. Despite strong mCherry expression, EGFP expression downstream of *mut-eR3-Nhlh*::EGFP* was abolished in five of the seven embryos or restricted to a few non-commissural neurons in two of the seven embryos (fig. S9F). This result indicates that *eR3-Nhlh* enhancer activity drives gene activation pattern similar to *Robo3* expression, and this activity depends on intact Nhlh1/2 binding sites. We further performed the reporter assay in mouse midbrains. Although E14.5 mouse midbrains showed undetectable level of endogenous Robo3 (Fig. 1C), we found moderate activity of *eR3-Nhlh*::EGFP* at E14.5 (fig. S9G), which might be due to an absence of inhibitory regulatory elements in the reporter construct that are otherwise present in the endogenous *Robo3* upstream sequences. The moderate enhancer activity, however, is up-regulated by co-EP of *Nhlh1/2-fl* (fig. S9, H and K). Notably, *mut-eR3-Nhlh*::EGFP* showed no or low activity both alone and when co-electroporated with *Nhlh1/2-fl* (fig. S9, I to K), indicating that the enhancer activity depends on the integrity of Nhlh1/2 binding sites. The in vivo reporter assay results supported the notion that Nhlh1/2 binding to *eR3-Nhlh* via their binding sites mediates the transactivation of *Robo3* expression.

Isl1 negatively regulates Robo3 induction by Nhlh1 and Nhlh2

Our expression studies, in both mice and chick, showed that *Nhlh1* and *Nhlh2* combined expression area was wider than that of *Robo3*. In the spinal cord, *Nhlh1* and *Nhlh2* were clearly expressed in the part of the ventral spinal cord including the MN domain, which is devoid of *Robo3* expression (Figs. 3B and 6B). This poses a specificity problem for the Nhlh1/2-dependent specification of commissural neurons, prompting us to hypothesize that Nhlh1/2 activity might be subjected to negative regulation in certain neuron classes or subclasses. To begin to uncover such region-specific regulators, we turned to the developing spinal cord as a model due to the wealth of knowledge available on the molecules that define each cardinal spinal class and on its axon laterality (Fig. 7A) (*1*, *3*, *5*, *7*, *56*). We noticed that two ipsilaterally projecting neuron classes, namely, MNs and dI3 neurons, share the expression of Isl1, a LIM-HD TF. A previous study in chick spinal cord showed that ectopic expression of Isl1 in the contralaterally projecting dI1 neurons is sufficient to turn them into ipsilateral projection without affecting the cell fate (*57*). Therefore, we hypothesized that Isl1 might suppress Robo3 induction by Nhlh1/2. We tested this hypothesis using the midbrain paradigm. As in Fig. 1, forced expression of *Nhlh1/2* robustly activated Robo3 in the midbrain (Fig. 7, C and D). We then co-electroporated wild-type *Isl1* (*Isl1-wt*) into the midbrain together with *Nhlh1*/2 and detected a marked suppression of Robo3 induction (Fig. 7, C and D). We next probed into the molecular nature of the Isl1-mediated suppression. To this end, we constructed three variants of Isl1 and assessed their effect on Nhlh1/2 activity (Fig. 7B): (i) Isl1-N231S: an amino acid substitution from asparagine (N) to serine (S) in Isl1 HD domain, resulting in a mutant form unable to bind DNA (*58*); (ii) Isl1-ΔLim: a deletion of the two LIM domains that prevent the binding of its obligatory cofactor Ldb1 and hence disrupt the formation of an effective transcriptional complex (*58*, *59*); (iii) Isl1-ΔLBD: a deletion of the LIM-binding domain (LBD) in the C-terminal of Isl1 abolishing its ability to interact with Lhx3 (*60*). Both Isl1-N231S and Isl1-ΔLim failed to suppress Nhlh1/2-mediated induction of Robo3, whereas Isl1-ΔLBD could suppress (Fig. 7, C and D). The successful expression of the electroporated constructs was demonstrated by Isl1 IHC (fig. S10A). This result suggests that Isl1 suppresses Nhlh1/2-mediated Robo3 induction as an HD TF that depends on the formation of Ldb1-Isl1 tetramer without recruitment of additional LIM-HD TFs.

We next investigated whether Isl1 can suppress endogenous Robo3 expression and impose ipsilateral projection fate. *Isl1* was electroporated unilaterally into the chick spinal cord, and Robo3 expression was compared between the electroporated and non-electroporated sides after Robo3 IHC and ISH. We detected a marked reduction of endogenous Robo3 level by Isl1 expression (Fig. 7E and fig. S10B). Furthermore, by electroporating *Isl1* with *EGFP*, we were able to follow the axon trajectories at the ventral midline. We found that EP of *Isl1* with *EGFP* markedly reduced the number of axons at the ventral midline, in comparison with the abundant midline axons in samples electroporated with *EGFP* alone (Fig. 7F and fig. S10C). For mouse spinal cord, due to technical difficulties of in utero EP at younger stages, we performed EP at E11.5 at which stage most neurons labeled were of the two later born spinal classes dILA and dILB (*3*). The small percentage of neurons accessible to EP labeling made it difficult to examine Robo3 down-regulation as what had been done in chick. We therefore examined the effect of Isl1 on the laterality of labeled axons. We found that similar to that in chick, Isl1 expression in mouse spinal cord led to a marked reduction of axons arriving at and crossing the midline (Fig. 7G and fig. S10D). Together, these results identified Isl1 as a negative regulator that suppresses Robo3 expression, suggesting that Isl1 might act regionally to render specificity to the specification of commissural neurons.

DISCUSSION

Here, we uncovered a common gene regulatory program for the specification of contralateral axon projections in all FP-crossing commissural neurons in mice. Mechanistically, Nhlh1 and Nhlh2 function redundantly to activate the guidance receptor Robo3 via binding to Nhlh1/2 binding sites in a *Robo3* enhancer. The Nhlh1/2-mediated regulation of Robo3 expression might be conserved in chick. We further showed that LIM-HD TF Isl1 negatively regulates Robo3 expression induced by Nhlh1/2. Our findings shed light on a strategy in which a conserved globally acting mechanism intersects with class or subclass-specific regulators to control the partition of neurons into commissural and ipsilateral projection categories.

The way Nhlh1/2 regulate Robo3 expression is via binding to the Nhlh1/2 binding sites identified in a distal enhancer element of *Robo3* genomic locus as demonstrated by ChIP-qPCR and in vivo reporter assays. Nhlh1/2 have been suggested to act either as an activator or repressor (*30*, *42*–*44*), perhaps depending on the nature of the cofactors associated with them. We showed that Nhlh1/2 serve as activators with respect to Robo3 induction by using VP16 and EnR fusions. Nhlh1/2 belong to the TAL1/SCL subfamily of class II bHLH TFs (*39*, *40*). As with all bHLH TFs, the HLH domain mediates protein interactions, and the basic domain directs DNA binding

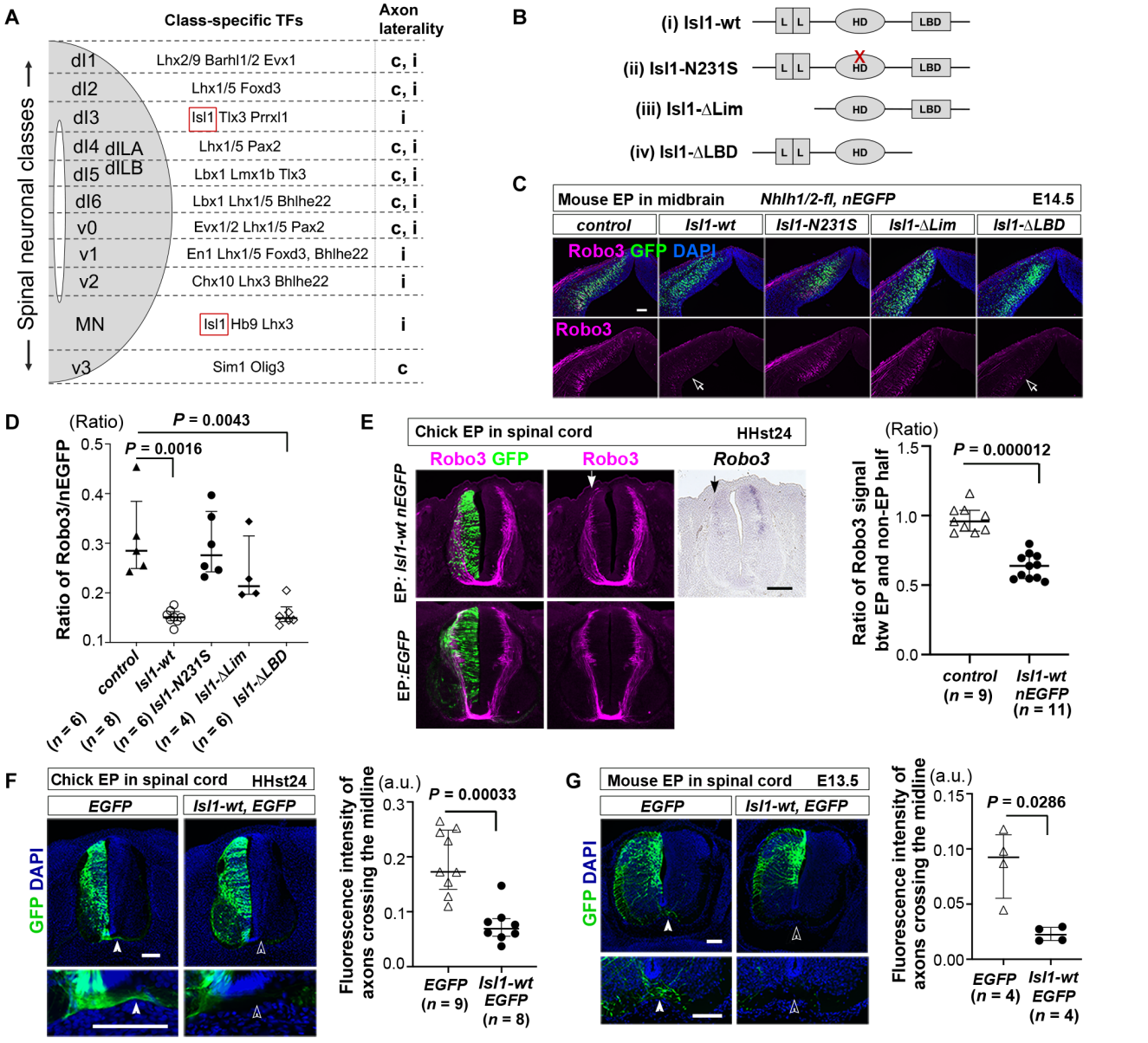

Fig. 7. Isl1 negatively regulates Nhlh1/2-mediated Robo3 induction and commissural axon specification. (**A**) A schematic summarizing the cardinal spinal neuron classes, the unique combination of TFs that characterize each class, and their axon laterality. c, commissural; i, ipsilateral. Red boxes, Isl1 expression in dI3 and MN classes. (**B**) A schematic showing the domain structures of the four Isl1 constructs in (C). (**C**) In utero EP in mouse midbrains with constructs indicated above each image. Ectopic Robo3 induction by Nhlh1/2-fl is markedly suppressed when Isl1-wt or Isl1-ΔLBD was co-electroporated, but not Isl1-N231S or Isl1-ΔLim. (**D**) Quantification of the result in (C) by the ratio between the Robo3 and EGFP fluorescence within a ROI. (**E**) *Isl1-wt* with *nEGFP* (top) or *EGFP* alone (bottom) was electroporated into HHst16/17 chicken spinal cords and samples analyzed at HHst23/24 by IHC and ISH. The ratio between the Robo3 fluorescence on the EP over the non-EP side of the same section was quantified. (**F** and **G**) *EGFP* was electroporated, either with *Isl1-wt* or with an empty vector, into HHst16/17 chick (F) or E11.5 mouse (G) spinal cords to investigate the laterality of labeled axons at HHst24 and E13.5, respectively. Isl1 expression led to a marked reduction of axons crossing the ventral midline (hollow arrowhead) compared with the control (filled arrowhead) in both chick (F) and mouse (G). The fluorescence of axons at the ventral midline was measured within a ROI with fixed area and normalized to the level of EP measured by the GFP signal within the dorsal half of the spinal cord. All quantitative data in (D) to (G) were represented by a scatter plot with lines marking the median and upper and lower quantiles, and the statistical analyses were performed using Mann-Whitney *U* test. a.u., arbitrary units. Scale bars, 100 μm [(C) and (E) to (G)].

(*48*). The highly charged R6 domain unique to Nhlh1/2 together with the adjoining canonical basic domain was speculated to constitute an extended basic domain with a distinct binding specificity (*39*, *41*). We showed that the R6 domain is required for Robo3 induction, raising the possibility that Nhlh1/2 function might be irreplaceable by other bHLH families in Robo3 induction. The HLH domain of Nhlh1/2 is also indispensable for Robo3 induction because the *Nhlh1* mutant allele lacking the HLH domain fails to activate Robo3 (fig. S4, E and F), suggesting the necessity of dimerization with other proteins. Previous in vitro studies have shown that mouse

and human Nhlh1/2 can interact with a range of cofactors, including class I bHLH proteins (E12 and E47) and LIM-only proteins (Lmo1 to Lmo4), or homodimerize (*30*, *41*–*43*). What cofactors are functionally important in vivo awaits further investigations. Heterodimerization between Nhlh1 and Nhlh2, however, is not required for Robo3 induction in vivo because *Nhlh1* and *Nhlh2* single mutants show normal commissure formation.

Nhlh1/2 are expressed in postmitotic immature neurons (*27*, *39*) and are expected to regulate early neuronal differentiation. However, their function in neural development has remained largely obscure, perhaps, in part, due to their highly overlapped expression and functional redundancy. dKO of *Nhlh1/2* have been generated previously (*29*–*31*). Although the dKO mice die at birth (*29*, *50*), only two developmental defects have been reported thus far: migration defects in GnRH neurons and PN neurons (*30*, *31*). Neither of these defects could account for the perinatal lethality, suggesting more severe defects yet to be discovered. By generating *Nhlh1/2*-double-deficient mice, we found a complete lack of ventral commissures from the spinal cord to the midbrain. The commissure-less phenotype provides a satisfactory explanation for the perinatal lethality of these mice, as desynchronization of the respiratory oscillator owing to disrupted commissural connections in the hindbrain preBötzinger complex has been suggested as a cause of perinatal death in *Robo3* KO mice (*17*, *26*).

Are Nhlh1/2 sufficient to confer contralateral axon projection? In the midbrain, most neurons accessible to labeling by EP at E11.5 are ipsilaterally projecting neurons (*21*). We found that some of them could be driven to project contralaterally upon forced expression of Nhlh1/2. This finding is supported by similar observations in the hindbrain. However, the sufficiency of Nhlh1/2 in instructing axon laterality should be considered with caution. A previous study showed that mouse Robo3, via binding to DCC, promotes axon extension to the FP by potentiating Netrin-1 responsiveness of commissural axons (*19*). This implies that both Robo3 and DCC should be present to achieve maximum responsiveness to Netrin-1. Nhlh1/2 are unlikely to affect DCC expression as we did not detect notable changes in DCC expression in the double mutant (fig. S7, C and F). It is possible that the ectopic contralateral projection driven by Nhlh1/2 forced expression might come only from DCC-expressing neurons. We think that the sufficiency of Nhlh1/2 in driving contralateral axon projection should be discussed by considering the specifics of the cellular context.

A fundamental yet unresolved neurodevelopmental issue is whether the specification of shared traits in divergent classes of neurons is determined by common regulatory mechanisms or whether they are separately regulated. The same neurotransmitter phenotype appears to be regulated by different gene regulatory programs that act on distinct cis-regulatory elements in different neuron classes (*3*, *61*). Commissural axon projection is a trait imposed during development on heterogenous classes of neurons (*4*, *7*). Take the mouse spinal cord for example, 8 of the 13 cardinal spinal classes (dI1, dI2, dI4, dI5, dI6, dILA, dILB, and V0) contain a mixture of contralateral and ipsilateral projecting neurons (*1*, *3*, *7*). Before this study, no common regulatory mechanism has been found to control Robo3 expression and commissural axon projection (*4*, *62*). Our findings here proved the existence and identified the nature of such a common mechanism. Nhlh1/2 work as a master regulator of Robo3 globally from the spinal cord to the midbrain for all the FP-crossing commissural neurons (Fig. 8), and this mechanism is conserved in chick. Phylogenetic analysis of Nhlh1 and Nhlh2 showed that both genes exist prevalently across vertebrate lineages but not in invertebrates, and one of the two paralogs is present in Lamprey, the ancestral vertebrate. It is tempting to speculate that the three events: the emergence of the FP, the deployment of Robo3 for contralateral axon projections across the FP, and the recruitment of Nhlh1/2 to transactivate Robo3 expression, might have coevolved from an early point during the vertebrate evolution.

While Nhlh1/2 are absolutely required for Robo3 induction in commissural neurons, they cannot be the sole determinant of commissural projection trait because they are also expressed in neurons that are Robo3-negative, such as the spinal MNs. We hypothesized that negative regulators of Robo3 expression must exist to confine Robo3 expression, and we provided evidence that Isl1 serves as such a negative regulator. As a consequence, ectopic Isl1 expression suppresses contralateral axon projections in both chick and mice spinal cord, in line with a previous study in chick (*57*). It is one of the limitations of this study that we still do not know how Isl1 exerts this repressive function except as an HD TF. Isl1 could potentially antagonize Nhlh1/2 activity by directly converging onto *Robo3* enhancer/promoter or indirectly via either activating a repressor or repressing an activator of Robo3 expression. Another limitation of this study is that at present we do not know whether Isl1 is essential to keep Robo3 expression out of the ipsilateral MN and dI3 neurons. Future studies are needed to address these limitations.

We think that, besides Isl1, Nhlh1/2-mediated Robo3 expression is almost certain to be subjected to other additional region-specific regulators for the following reasons. (i) Nhlh1/2 also appear to be expressed in V1 and possibly V2 spinal neurons. Both are primarily ipsilateral-projecting and Robo3-negative but do not express Isl1 (*1*), suggesting the existence of other negative regulators of Robo3 in these neurons. (ii) Lhx2/9 dKO phenotype suggests that these molecules are required for Robo3 expression in spinal dI1 neurons (*25*). The requirement of both Lhx2/9 and Nhlh1/2 for Robo3 expression in dI1 neurons suggests that the two groups of TFs may cooperate to achieve Robo3 activation possibly via binding to their respective cis-regulatory regions on the *Robo3* genomic locus. A recent study identified an enhancer element 20 kb upstream of the *Robo3* transcriptional start site that is conserved across vertebrates (*63*). They showed that a reporter gene expression driven by this enhancer element in chick spinal cord overlap with Robo3 expression and also overlap with Lhx1 expression. Given that Lhx1/5 are expressed in commissural neuron-containing dI2, dI4, dI6, and V0 spinal neurons, it is tempting to speculate that Robo3 expression in these neuron classes other than dI1 might rely on cooperation between Nhlh1/2 and Lhx1/5. We propose a model that depicts the mechanism underlying the binary partitioning of neurons into commissural and ipsilateral groups (Fig. 8). The presence of Nhlh1/2, possibility facilitated by coactivators, defines the commissural projection neurons. On the other hand, either the absence of Nhlh1/2 or their suppression by repressors (such as Isl1) defines the ipsilateral projection neurons. It is becoming increasingly clear, supported by single-cell transcriptomics, that the lineage-defined cardinal spinal classes could be further diversified into dozens of functionally or molecularly distinct subclasses (*56*, *64*–*67*). How the axon laterality-based division aligns with newly defined neuronal subclasses is still little understood. It would be of future interest to examine how Robo3 expression is regulated at single-cell

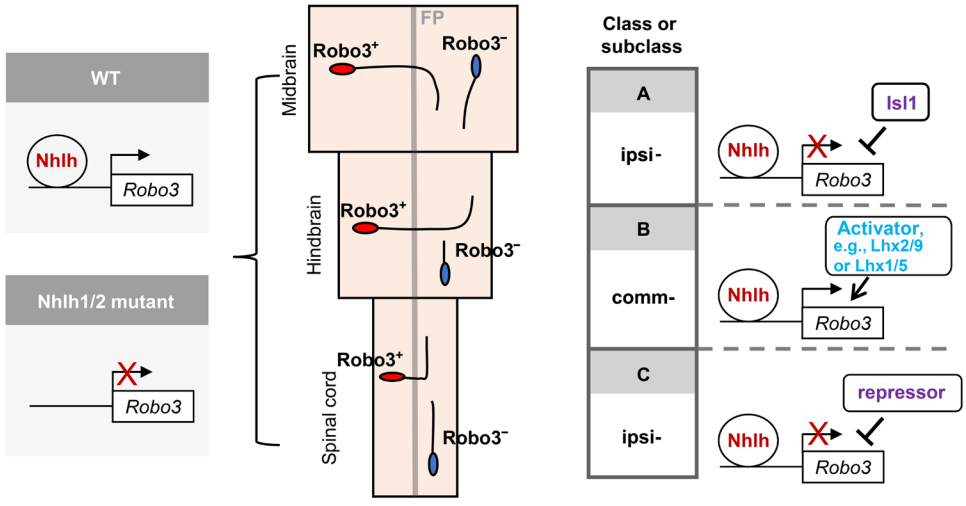

Fig. 8. A model summarizing the findings of this study. ipsi-, ipsilateral projecting neurons; comm-, commissural neurons. WT, wild type.

resolution within the neuron classes that contain a mixture of commissural and ipsilateral neurons to gain insights into mechanisms that control the ratio of these two types of neurons. Such fine-grained regulation of Robo3 within a neuron class may take place by modulating Nhlh1/2 activity and hence can be interrogated within the framework generated by this study.

MATERIALS AND METHODS

Animals

For expression studies with ISH and in utero EP, timed pregnant ICR mice (Japan SLC, Shizuoka, Japan) were used. Noon of the day on which a vaginal plug was detected was designated as E0.5. *Nhlh1* and *Nhlh2* mutant mouse lines, initially on a B6C3F1 hybrid background, were backcrossed to C57BL/6J for at least four to five generations before phenotype analyses to minimize potential off-target effects by CRISPR-Cas9 gene editing. Double and single heterozygotic colonies were maintained. To generate double homozygotic embryos, double heterozygotic male and female mice were crossed. Genotyping were performed on tail lysis using the following primers: Nhlh1-geno-F and Nhlh1-geno-R for *Nhlh1* mutant; and Nhlh2-geno-F, Nhlh2-geno-F-2, Nhlh2-geno-R, and Nhlh2-geno-R-2 for *Nhlh2* mutant. Sequences of these primers are listed in table S1. For bulk RNA-seq experiment, transgenic mouse line Tg(Barhl1-EGFP)GS25Gsat (the Jackson Laboratory, MGI ID:4846878) was used for obtaining pure PN populations.

For chick embryos, fertilized white leghorn eggs (Ohata Shaver Hatchery, Shizuoka, Japan; or Gil-Guy Farm, Israel) were incubated in a humidified incubator at 38°C to desired stages. Staging of chick embryos follows the Hamburger and Hamilton (HH) stage (st) series (*68*).

All animal maintenance and manipulations were carried out in accordance with the Japanese guidelines and regulations (2006) for scientific and ethical animal experimentation and were approved by the National Institute of Genetics, Japan, and Kansai Medical University, Japan, or with the designated policies of the Experiments in Animals Ethics Committee of the Hebrew University and were performed with its approval.

DNA constructs

Expression constructs *pCAG-EGFP* and *pCAG-mCherry* and *pCAG-nls-EGFP* (a gift from Y. Tanabe, Kyoto University, Japan) contain enhanced GFP (EGFP), mCherry, and nls-EGFP (nucleus-localized EGFP) open reading frames in pCAGGS vector, respectively. Full-length (fl) *Nnlh1* and *Nhlh2* expression constructs were constructed by PCR amplification of the coding sequences of *Nhlh1* (GenBank, accession NM_010916) and *Nhlh2* (GenBank, accession NM_178777) from mouse E11.5 brain cDNA using the primer pairs: Nhlh1-fl-F and Nhlh1-fl-R, and Nhlh2-fl-F and Nhlh2-fl-R. The PCR products were cloned into a *pCAGGS* vector with a multiple cloning site inserted to generate *pCAG-Nhlh1-fl* and *pCAG-Nhlh2-fl*. The PCR products were also cloned into a *pCAG-2HAN* plasmid that contains the *pCAGGS* backbone with two HA tags at the N terminus. This resulted in the generation of fusion proteins of Nhlh1 and Nhlh2 with two HA tags at their N termini. To produce VP16 or EnR fusion of Nhlh1- and Nhlh2-fl, the *VP16* and *EnR* coding sequences were excised from *pCS2 + NLSVP16AD* and *pCS2 + EnR* plasmids (gifts from M. Hibi, Nagoya University, Japan) (*69*), respectively, and cloned into *pCAG-Nhlh1-fl* and *pCAG-Nhlh2-fl* at 5′ to and in frame with *Nhlh1* and *Nhlh2* coding sequences. To construct the *pCAG-bHLH1-VP16* and *pCAG-bHLH2-VP16* constructs, the bHLH domains (excluding the R6) of *Nhlh1* and *Nhlh2* were PCR-amplified with a forward primer, Nhlh-bHLH-F, for both *Nhlh1* and *Nhlh2*, and reverse primers: Nhlh1-fl-R for *Nhlh1* and Nhlh2-fl-R for *Nhlh2*. To construct *pCAG-R6-bHLH1-VP16* and *pCAG-R6-bHLH2-VP16*, the R6-bHLH domains, from *Nhlh1* and *Nhlh2*, were PCR-amplified with primer pairs: Nhlh1-R6-bHLH-F and Nhlh1-fl-R, and Nhlh2-R6-bHLH-F and Nhlh2-fl-R, respectively. The PCR fragments were cut with Xho I and Not I and were subcloned into Xho I– and Not I–digested *pCAG-Nhlh1-VP16* and *pCAG-Nhlh2-VP16* plasmids to replace the full-length *Nhlh1* and *Nhlh2*, respectively. *Nhlh1/2-fl-EnR* and *bHLH1/2-VP16* were also cloned into a *pCAG-2HAC* plasmid that contains the *pCAGGS* backbone with two *HA* tags at the C terminus. This resulted in the generation of *Nhlh1/2-fl-EnR-HA* and *bHLH1/2-VP16-HA*. The wild-type *Isl1* expression construct was constructed by PCR amplification of the coding sequences of *Isl1* (GenBank, accession NM_021459) from mouse E11.5 brain cDNA

using primers: Isl1-wt-F and Isl1-wt-R. The PCR product was cloned into a *pCAGGS* vector with a multiple cloning site inserted to generate *pCAG-Isl1-wt*. To generate *pCAG-Isl1-N231S*, site directed mutagenesis was performed on *pCAG-Isl1-wt* so that the amino acid at the 231st position was changed from asparagine (N) to serine (S) using the following primers: Isl1-N231S-F and Isl1-N231S-R. To generate *pCAG-Isl1-ΔLim*, an N-terminal truncated Isl1 was amplified using the following primers: Isl1-dLim-F and Isl1-wt-R. To generate *pCAG-Isl1-ΔLBD*, a C-terminal truncated Isl1 was amplified using the following primers: Isl1-wt-F and Isl1-dLBD-R. The PCR products were cloned into the pCAGGS vector as above. The *Lhx2* expression construct was constructed by PCR amplification of the coding sequences of *Lhx2* (GenBank, accession NM_010710) from mouse E11.5 brain cDNA using primers: mLhx2-F and mLhx2-R. The PCR product was cloned into a *pCAGGS* vector with a multiple cloning site to generate *pCAG-Lhx2*. All the cloned expression constructs were confirmed by sequencing.

For generating in vivo GFP reporter constructs driven by Robo3 regulatory sequences for chick spinal cord and mouse midbrain EP, a 1090–base pair (bp) *eR3-Nhlh* (GRCm38/mm10, chr9:37,460,015-37,461,104) enhancer and a 565-bp promoter/5′UTR (GRCm38/mm10, chr9:37,433,002-37,433,566) fragments were cloned in tandem 5′ to EGFP to make *eR3-Nhlh::EGFP*. To mutate Nhlh1/2 binding sites in *eR3-Nhlh::EGFP*, the sequence-altered enhancer region was ordered as gBlocks Gene Fragments (Integrated DNA Technologists, Coralville, Iowa). Because of the high GC content within *eR3-Nhlh* region that prevents DNA synthesis, five short (3 to 6 bp) stretches of GC were converted to AT, either without mutating the Nhlh1/2 binding sites, designated as *eR3-Nhlh*::EGFP*, or with the four E-box core elements of the Nhlh1/2 binding sites mutated, designated as *mut-eR3-Nhlh*::EGFP* (fig. S9B).

Constructs for generating riboprobes to detect mouse *Robo3*, *Nhlh1*, *Nhlh2*, and *Netrin-1* and chick *Robo3*, *Nhlh1*, and *Nhlh2* were made using the pGEM-T Easy vector system (Promega) by PCR amplification from mouse E11.5 brain cDNA or HHst24 chick cDNA with the following primer pairs: mRobo3-ISH-F and mRobo3-ISH-R for mouse *Robo3*, mNhlh1-ISH-F and mNhlh1-ISH-R for mouse *Nhlh1*, mNhlh2-ISH-F and mNhlh2-ISH-R for mouse *Nhlh2*, and mNetrin-1-ISH-F and mNetrin-1-ISH-R for mouse *Netrin-1*, cRobo3-ISH-F and cRobo3-ISH-R for chick *Robo3*, cNhlh1-ISH-F and cNhlh1-ISH-R for chick *Nhlh1*, and cNhlh2-ISH-F and cNhlh2-ISH-R for chick *Nhlh2*. *VP16* and *EnR* ISH probes were prepared by using primer pairs VP16-ISH-F and VP16-ISH-R (T7 containing) for *VP16* and EnR-ISH-F and EnR-ISH-R (T7 contianing) for *EnR* riboprobes. Sonic hedgehog (*Shh*) riboprobe was a gift from T. Shiroishi and T. Sagai (National Institute of Genetics, Japan) (*70*).

For generating single guide RNA (sgRNA) for gene editing in fertilized mouse eggs, oligonucleotide pairs were annealed and cloned into Bbs I–digested *pX330* (Addgene, plasmid no. 42230) (*71*): Nhlh1-sgRNA1-F and Nhlh1-sgRNA1-R for *Nhlh1-sg1*; Nhlh1-sgRNA2-F and Nhlh1-sgRNA2-R for *Nhlh1-sg2*; Nhlh2-sgRNA1-F and Nhlh2-sgRNA1-R for *Nhlh2-sg1*; and Nhlh2-sgRNA2-F and Nhlh2-sgRNA2-R for *Nhlh2-sg2*. Sequences of all oligonucleotides were listed in table S1.

Bulk RNA-seq experiment

Using Tg(Barhl1-EGFP) mouse line that expresses EGFP in most PN neurons during and after their migration, we dissected out migrating PN neurons at E14.5 and PN neurons in their final PN nuclei region at E18.5. The tissue pieces were dissociated into single cells by Papain dissociation following a procedure resembling that of Worthington's papain dissociation system. EGFP-expressing PN neurons were then enriched by fluorescence-activated cell sorting (Cell Sorter SH800, SONY) and total RNA prepared by the RNeasy Plus Micro Kit (Qiagen, 74034). Samples from five biological replicates at either E14.5 or E18.5 were subjected to mRNA selection and cDNA preparation (KAPA mRNA HyperPrep Kit, KAPA BIOSYSTEMS, KR1352) and to next-generation sequencing on an Illumina HiSeq2500 platform. Between 25 and 29 million 100-bp paired-end reads per sample were obtained.

Generation of *Nhlh1* and *Nhlh2* mutant mice

The CRISPR-Cas9 guide sequences for *Nhlh1* and *Nhlh2* genes were selected using CRISPOR (http://crispor.tefor.net) (*72*) and CRISPRdirect (http://crispr.dbcls.jp) (*73*) webtools (fig. S4A). The sgRNAs were synthesized as reported previously (*74*). B6C3F1 (C57BL/6N × C3H/HeN) female mice were superovulated and mated with B6C3F1 males, and fertilized eggs were collected from oviducts. The synthesized sgRNAs (50 ng/μl) and TrueCut Cas9 protein v2 (100 ng/μl; Invitrogen) were premixed in Opti-MEM (Thermo Fisher Scientific) and electroporated into fertilized eggs using CUY21EDIT II electroporator and LF501PT1-10 platinum plate electrode (BEX Co. Ltd.) following the method reported previously (*75*). The electroporated zygotes were cultured in KSOM mouse embryo media (Merck Millipore) at 37°C under 5% CO_2 until the two-cell stage after 1.5 days. Thereafter, 20 to 32 two-cell stage embryos were transferred into the uterus of pseudopregnant Multi-Cross Hybrid females at 0.5 days after coitum. Founder mice were screened for edited *Nhlh1* and *Nhlh2* alleles that were subsequently sequenced to obtain the precise nature of the edited alleles. Two founder lines were then chosen for breeding, backcrossing, and analyses (fig. S4, C and D).

In vivo EP

The pregnant mice were anesthetized either with a combination of isoflurane (1.0% in air) and pentobarbital sodium (80 mg/kg body weight; Somnopentyl, Kyoritsu Seiyaku Corporation, Tokyo, Japan) or with a mixture of medetomidine (37.5 μg/kg; Nippon Zenyaku Kogyo, Fukushima, Japan), midazolam (2 mg/kg; Sandoz, Tokyo, Japan), and butorphanol (0.25 mg/kg; Meiji Seika Pharma, Tokyo, Japan). The uterus was exposed after abdominal incision, and ~2 μl of plasmid was injected into the 4th ventricle, the central canal of the spinal cord, or the cerebral aqueduct of E12.5 or E11.5 embryos. Five square electric pulses (30 V, 50-ms duration at 200-ms intervals) were applied using a forceps-type electrode (CUY650P5 or CUY650P2, Nepa Gene, Japan) connected to a square-pulse generator (CUY21, BEX, Japan).

In ovo EP was performed on HHst16/17 chick embryos essentially as previously described with some modifications (*76*). Approximately 0.5 μl of DNA solution at 1 to 2 μg/μl (or in the case of reporter analysis at 5 μg/μl) was injected into the central canal of the spinal cord, and three square electric pulses (25 V, 50-ms duration at 950-ms intervals) were applied using either a parallel platinum electrode (4-mm exposed end and 0.5-mm diameter) connected to a square-pulse generator (CUY21, BEX, Japan) or a 0.5-mm tungsten wire electrode connected to a BTX electroporator (ECM 830).

Tissue processing and sectioning

Pregnant mice were killed by cervical dislocation, and embryos were taken out from the uterus. Chick embryos were removed from eggs. Mouse brains and spinal cords and chick spinal cords were dissected out in phosphate-buffered saline (PBS; pH7.4) and fixed in 4% paraformaldehyde (PFA) in 0.01 M PBS at 4°C for 4 to 7 hours. The tissues were then cryo-protected in 30% sucrose in PBS overnight at 4°C and embedded in optimal cutting temperature compound (Sakura FineTek, Japan). Frozen sections of 20-μm thickness were obtained with a cryostat (Leica CM3050S).

ISH on sections

Riboprobes were prepared using the digoxigenin (DIG) RNA labeling mix (Roche, 11277073910). Tissue sections were pre-hybridized at 65°C for 2 hours in hybridization buffer composed of 50% formamide (deionized and nuclease tested, Nacalai Tesque), 1.3× saline-sodium citrate buffer (SSC), 1× Denhardt's solution (Wako), yeast tRNA (0.1 mg/ml), and 10% (w/v) dextran sulphate (M_w of 500,000; Merck Millipore). The sections were then incubated with hybridization buffer containing anti-sense riboprobe (1.5 μg/ml) at 65°C overnight. The next day, sections were washed twice at 65°C with formamide wash buffer (50% formamide, 1× SSC, and 0.1% Tween 20) and then twice at room temperature (RT) with 1× MABT (100 mM maleic Acid, 150 mM NaCl, and 0.1% Tween 20). Blocking was performed in 1× MABT with 2% blocking reagents (Roche) and 10% donkey serum (Sigma-Aldrich) for 1 hour at RT and reacted with anti–DIG-AP Fab fragments (Roche, 11093274910; 1:1500) in the blocking solution at 4°C overnight. The next day, slides were washed three times in 1× MABT and rinsed once in NTMT solution [0.1 M tris-HCl (pH 9.5), 0.1 M NaCl, 0.05 M MgCl2, and 0.1% Tween 20], and, then, color developing was carried out in NTMT containing nitro blue tetrazolium (100 μg/ml) and bromochloroindolyl phosphate (50 μg/ml).

Double-fluorescence ISH was performed essentially as previously described (*77*) with some modifications. *Nhlh2* and *Robo3* probes were prepared using DIG RNA labeling mix and fluorescein RNA labeling mix (Roche, 11685619910), respectively. Transverse sections of E11.5 spinal cords were incubated with a hybridization buffer containing *Nhlh2* and *Robo3* riboprobes at 60°C overnight. *Robo3* signals were first analyzed by incubation with peroxidase-conjugated anti-fluorescein antibody (Merck,11426346910; 1:500) followed by fluorescence detection using tyramide-conjugated fluorescein (PerkinElmer, NEL741001KT; 1:75). Subsequently, the sections were incubated with PBS containing 2% H_2O_2 for 30 min to inactive peroxidase activities derived from the peroxidase-conjugated anti-fluorescein antibody. *Nhlhl2* signals were then analyzed by incubation with peroxidase-conjugated anti-DIG antibody (Merck, 11207733910; 1:500) followed by fluorescence detection using tyramide-conjugated Cy3 (PerkinElmer, NEL744001KT; 1:75). The sections were counterstained with 0.03% 4′,6-diamidino-2-phenylindole (DAPI; Nacalai Tesque)

Immunohistochemistry

Tissue sections were blocked with 10% donkey serum (Sigma-Aldrich) in PBSTx (0.2% Triton X-100) for 1 hour at RT followed by incubation with primary antibodies at 4°C overnight. After washing with PBSTx, the sections were then incubated with the secondary antibodies at RT for 2 hours. In the case of Lhx1 IHC, the slides were first subjected to antigen retrieval by HistoVT One (Nacalai Tesque) following the manufacturer's instruction and then underwent the general IHC process described above. Slides were counterstained with DAPI. The primary antibodies used were rabbit anti-Barhl1 polyclonal antibody (Atlas Antibodies; HPA004809, Sigma-Aldrich; 1:500), goat anti-Robo3 polyclonal antibody (R&D Systems, AF3076; 1:200), goat anti-Tag1 polyclonal antibody (R&D Systems, AF4439; 1:500), mouse anti–NF-160kD monoclonal antibody (clone RMO-270; Thermo Fisher Scientific, 13-0700; 1:500), rat anti-L1CAM monoclonal antibody (clone 324; Merck Millipore, MAB5272; 1:400), goat anti-DCC polyclonal antibody (Santa Cruz Biotechnology, sc-6535; 1:200), rabbit anti-FoxP2 polyclonal antibody (Abcam, ab16046; 1:1000), mouse anti-Brn3a monoclonal antibody (clone 5A3.2; Merck Millipore, MAB1585; 1;200), rabbit anti-Lim1/Lhx1 antibody (Abcam, ab229474; 1:250), rabbit anti-Lhx2 (Invitrogen, PA5-78287; 1:250), rat anti-HA (Roche; clone3F10; 1:100), guinea pig anti-Isl1 antibody (a gift from Y. Tanabe, Kyoto University, Japan), and chick anti-GFP polyclonal antibody (Abcam, ab13970; 1:1500). The secondary antibodies used were Cy3-donkey anti-rabbit immunoglobulin G (IgG) (Jackson ImmunoResearch, 1:300) for Barhl1, FoxP2, Lhx1, and Lhx2 antibodies; Cy3-donkey anti-goat IgG (Jackson ImmunoResearch, 1:300) for Robo3, Tag1, and DCC antibodies; Cy3-donkey anti-mouse IgG (Jackson ImmunoResearch, 1:300) for NF and Brn3a antibodies; Cy3-donkey anti-rat IgG (Jackson ImmunoResearch, 1:300) for an L1CAM antibody; Alexa Fluor 488–donkey anti-chick IgY (Jackson ImmunoResearch, 1:400) for a GFP antibody; and Alexa Fluor 647–donkey anti-guinea pig-IgG (Jackson ImmunoResearch 1:400) for Isl1 antibody.

ChIP real-time qPCR assay

E14.5 midbrains electroporated with *Nhlh1/2-fl* and *nEGFP* 2 days earlier were dissected out in cold PBS, and the GFP-positive tissues were collected and quick frozen in liquid nitrogen. ChIP assays were performed using the SimpleChIP Plus Enzymatic Chromatin IP Kit (Magnetic Beads) (Cell Signaling Technology, no. 9005) essentially following the manufacturer's instruction with the following modifications. Cross-linking was performed with 16% methanol-free formaldehyde solution (Thermo Scientific, ref. 28906) at a final concentration of 1.5%, and disaggregation of tissue was performed with a handheld homogenizer (Dispergierantrieb T 10 basic, at 30,000 rpm for 45 s). ChIP grade anti-HA tag antibody (Abcam, ab9110) or normal rabbit IgG (Cell Signaling Technology, no. 2729) was used at 3 μg per immunoprecipitation reaction. Purified DNA was subjected to real-time qPCR to detect quantitatively four genomic regions using the KAPA SYBR Fast qPCR kit (NIPPON Genetics, KK4601) on a Bio-Rad CFX96 Touch Real-Time PCR detection system. The four genomic regions, namely, *eR3-Nhlh-r1*, *eR3-Nhlh-r2*, *Robo3-7979*, and *DCC-2660*, were amplified using the following four pairs of primers: (i) *eR3-Nhlh-r1-F* and *eR3-Nhlh-r1-R*, (ii) *eR3-Nhlh-r2-F* and *eR3-Nhlh-r1-R*, (iii) *Robo3-7979-F* and *Robo3-7979-R*, and (iv) *DCC-2660-F* and *DCC-2660-R* (for sequences, see table S1), and the respective coordinates of the four genomic regions (GRCm38/mm10) are (i) chr9:37,460,700-37,460,799, (ii) chr9:37,460,700-37,460,918, (iii) chr9: 37,440,868-37,441,093, and (iv) chr18: 72,353,058-72,353,155. The ChIP efficiency was calculated using the percentage of input method.

In silico analysis of *Robo3* regulatory region

The regulatory region of mouse *Robo3* was analyzed using built-in tools in UCSC Genome Browser (http://genome.ucsc.edu) (*35*).

Robo3 locus was located on the mouse genome (assembly GRCm38/mm10), and its upstream sequences together with the first exon were scanned for potential regulatory elements using the "ENCODE cCREs (Candidate Cis-Regulatory Elements)" track (*78*). The degree of conservation of these potential regulatory elements across vertebrates was evaluated with the browser's "Vertebrate Multiz Alignment and Conservation" track. Each of these elements was then scanned for potential TFs binding sites using the "JASPAR Transcription Factors" track of the browser.

Building a phylogenetic tree of Nhlh1 and Nhlh2

The Nhlh1 and Nhlh2 protein sequences of species representing major vertebrate lineages were obtained from the protein database by National Center for Biotechnology Information. The absence of Nhlh1 and Nhlh2 orthologs in non-vertebrates were confirmed using the BLAST function. Multiple sequence alignment was performed on these sequences using MAFFT version 7 (https://mafft.cbrc.jp/alignment/software/) (*79*). The alignment was then fed into Molecular Evolutionary Genetics Analysis (MEGA 11) software for phylogenetic analysis and tree building (*80*). The amino acid substitution model used was Jones-Taylor-Thornton model. A phylogenetic tree was constructed using the maximum likelihood method, and the number of bootstrap replications was set at 500. The phylogenetic tree was rooted to Lamprey Nhlh1 because there are no Nhlh1 and Nhlh2 orthologs outside the vertebrates.

Image acquisition and processing

Fluorescence images on sections or flat-mounted brainstems were captured with a charge-coupled device camera (Axiocam, Zeiss) attached to an upright microscope (BX-60, Olympus) at 1296 × 1030 pixel resolution. Objective lens used were 2× Plan Apo with numerical aperture (NA) 0.08 (Olympus), 4× UPlan Apo with NA 0.16 (Olympus), 10× UPlan Apo with NA 0.40 (Olympus), and 20× UPlan Apo with NA 0.70 (Olympus). All bright-field images on ISH sections and some fluorescence images were captured with an All-in-one Fluorescence Microscope (BZ-X700, Keyence) with an objective lens of CFI 10× Plan Apo Lamda, NA 0.45 (Nikon), or CFI 20× Plan Apo Lamda, NA 0.75 (Nikon). Double-fluorescence ISH, triple-fluorescence IHC with HA, EGFP and Robo3, and Lhx1 IHC images were captured with a confocal laser scanning microscope (Olympus FV1200). Objective lens used were 20× UPlan SApo NA 0.75 and 40× UPlan SApo Sil NA 1.25. Adobe Photoshop CC and Adobe Illustrator CS3 were used to assemble figures.

Quantification and statistical analysis

For all experiments, the *n* numbers indicate the number of independent embryos analyzed. For quantifying the commissural index in the electroporated midbrains, fluorescence images of the whole-mounted brainstems were imported into ImageJ (National Institutes of Health, http://imagej.nih.gov/ij/). A region of interest (ROI) of a defined size encompassing the ipsilateral extending axons, the contralateral extending axons, and a background region on the sample were measured for its fluorescence level denoted as F_i, F_c, and F_b, respectively. For those control electroporated samples in which contralateral extending axons could not be easily visualized, the ROI was placed in a location mirroring the stereotypic location of the ectopic contralateral axon tract in the force-expressed samples. The commissural index was calculated as the percentage of commissural axons over the sum of ipsilateral and commissural axon tracts: $(F_c - F_b)/[(F_i - F_b) + (F_c - F_b)]$. For quantifying the midline crossing level in the electroporated hindbrains, fluorescence images of the hindbrain sections after IHC were imported into ImageJ. An ROI of defined size over a region just below the EP site, the FP region, and a background region on the sample were measured for its mean fluorescence level, denoted as F_{ep}, F_{fp}, and F_b, respectively. The GFP signal at the midline normalized by the strength of EP was calculated as $(F_{fp} - F_b)/(F_{ep} - F_b)$. To quantify the number of Brn3a-positive and Lhx1-positive neurons on the spinal cord samples, neurons with Brn3a or Lhx1 signals were manually counted on two to three sections for each sample and subsequently averaged. All the spinal cord sections used for quantification were of approximately equivalent axial levels. To quantify the effect of Isl1 on the induction of Robo3 by forced expression of *Nhlh1* and *Nhlh2*, the images of midbrain sections were imported to ImageJ. Background subtraction was first performed on each image using the subtract background function with rolling ball radius of 50.0 pixels, followed by placing an ROI of defined size over the electroporated area. Fluorescence of Robo3 and GFP of ROI were measured, and their ratio was taken to indicate the strength of Robo3 induction. Measurements of three sections from each sample were averaged to represent that sample. To quantify the suppression of endogenous Robo3 by *Isl1* EP in chick spinal cord, images were imported into ImageJ and background subtraction was performed as above. The mean fluorescence intensity of Robo3 signal within an ROI that encircles the dorsal half of spinal cord was measured for both the electroporated side and the non-electroporated side, and their ratio was taken as an indication of Robo3 suppression. Samples with EP of only EGFP were quantified in the same way. Measurements of three sections from each sample were averaged to represent that sample. To quantify the amount of midline crossing axons after *Isl1* EP in chick and mouse spinal cord, images were imported to ImageJ and background subtraction was performed as above followed by placing a rectangular ROI with fixed size at the ventral midline, and the GFP signal within the ROI was measured. This value was then normalized against the level of EP measured by the amount of GFP within an ROI that encircles the dorsal half of the spinal cord. Measurements of three sections from each sample were averaged to represent that sample. For all the above quantifications, data were represented by scatter plots with median and upper and lower quartiles indicated, and statistical analyses were performed by Mann-Whitney *U* test using Prism 8 (GraphPad). For quantifying the effect of EP of mutant *Nhlh1/2* into the mouse hindbrain and midbrain, after background subtraction as above, the mean fluorescence level within an ROI encircling the rhombic lip area, the electroporated midbrain area, or the cross sections of the migrating PN neurons on both the electroporated and the non-electroporated side of the same section were measured, and the ratio of the mean fluorescence levels between the electroporated and non-electroporated side was computed. Measurements of two sections from each sample were averaged to represent that sample. For quantifying the DCC expression level in the double mutant and control E16.5 PN neurons, after background subtraction as above, the cross section of the migrating PN stream was outlined, and the mean fluorescence level within the outlined region was measured. Measurements of two sections from each brain were averaged to represent that sample. The ratio of DCC fluorescence between the double mutant and the control was calculated. To quantify the activity of the Robo3 enhancer *eR3-Nhlh* in chick spinal cord, the amount of *CAG::mCherry* and *eR3-Nhlh*::EGFP*-labeled axons in the

ipsilateral and contralateral white matter of the spinal cord was measured by ImageJ using ROIs that encircled these regions. The percentage of commissural axons was calculated by dividing the commissural fluorescence into the combined fluorescence of both the ipsilateral and contralateral sides. The data were presented in a before-after plot. To quantify the activity of the *Robo3* enhancer *eR3-Nhlh* in mouse midbrain, the mean fluorescence intensity of GFP in a defined ROI on the EP side and the non-EP side was measured and subtracted. The subtracted value was then normalized by the mean fluorescence intensity of mCherry within the same ROI on the EP side. Measurement of four to six sections from each sample was averaged to represent that sample. The data were presented in a scatter plot with the line indicating the medians of each condition.

Supplementary Materials

This PDF file includes:

Fig. S1 to S10

Table S1

REFERENCES AND NOTES

1. W. A. Alaynick, T. M. Jessell, S. L. Pfaff, SnapShot: Spinal cord development. *Cell* **146**, 178–178.e1 (2011).
2. L. C. Greig, M. B. Woodworth, M. J. Galazo, H. Padmanabhan, J. D. Macklis, Molecular logic of neocortical projection neuron specification, development and diversity. *Nat. Rev. Neurosci.* **14**, 755–769 (2013).
3. H. C. Lai, R. P. Seal, J. E. Johnson, Making sense out of spinal cord somatosensory development. *Development* **143**, 3434–3448 (2016).
4. A. Chedotal, Development and plasticity of commissural circuits: From locomotion to brain repair. *Trends Neurosci.* **37**, 551–562 (2014).
5. P. J. Osseward II, N. D. Amin, J. D. Moore, B. A. Temple, B. K. Barriga, L. C. Bachmann, F. Beltran Jr., M. Gullo, R. C. Clark, S. P. Driscoll, S. L. Pfaff, M. Hayashi, Conserved genetic signatures parcellate cardinal spinal neuron classes into local and projection subsets. *Science* **372**, 385–393 (2021).
6. H. Zeng, J. R. Sanes, Neuronal cell-type classification: Challenges, opportunities and the path forward. *Nat. Rev. Neurosci.* **18**, 530–546 (2017).
7. A. J. Tulloch, S. Teo, B. V. Carvajal, M. Tessier-Lavigne, A. Jaworski, Diverse spinal commissural neuron populations revealed by fate mapping and molecular profiling using a novel Robo3(Cre) mouse. *J. Comp. Neurol.* **527**, 2948–2972 (2019).
8. A. Chedotal, Roles of axon guidance molecules in neuronal wiring in the developing spinal cord. *Nat. Rev. Neurosci.* **20**, 380–396 (2019).
9. J. D. Comer, S. Alvarez, S. J. Butler, J. A. Kaltschmidt, Commissural axon guidance in the developing spinal cord: From Cajal to the present day. *Neural Dev.* **14**, 9 (2019).
10. F. Friocourt, P. Kozulin, M. Belle, R. Suarez, N. Di-Poi, L. J. Richards, P. Giacobini, A. Chedotal, Shared and differential features of Robo3 expression pattern in amniotes. *J. Comp. Neurol.* **527**, 2009–2029 (2019).
11. V. Marillat, C. Sabatier, V. Failli, E. Matsunaga, C. Sotelo, M. Tessier-Lavigne, A. Chedotal, The slit receptor Rig-1/Robo3 controls midline crossing by hindbrain precerebellar neurons and axons. *Neuron* **43**, 69–79 (2004).
12. A. Tamada, T. Kumada, Y. Zhu, T. Matsumoto, Y. Hatanaka, K. Muguruma, Z. Chen, Y. Tanabe, M. Torigoe, K. Yamauchi, H. Oyama, K. Nishida, F. Murakami, Crucial roles of Robo proteins in midline crossing of cerebellofugal axons and lack of their up-regulation after midline crossing. *Neural Dev.* **3**, 29 (2008).
13. A. Okada, F. Charron, S. Morin, D. S. Shin, K. Wong, P. J. Fabre, M. Tessier-Lavigne, S. K. McConnell, Boc is a receptor for sonic hedgehog in the guidance of commissural axons. *Nature* **444**, 369–373 (2006).
14. F. Charron, E. Stein, J. Jeong, A. P. McMahon, M. Tessier-Lavigne, The morphogen sonic hedgehog is an axonal chemoattractant that collaborates with netrin-1 in midline axon guidance. *Cell* **113**, 11–23 (2003).
15. A. Fazeli, S. L. Dickinson, M. L. Hermiston, R. V. Tighe, R. G. Steen, C. G. Small, E. T. Stoeckli, K. Keino-Masu, M. Masu, H. Rayburn, J. Simons, R. T. Bronson, J. I. Gordon, M. Tessier-Lavigne, R. A. Weinberg, Phenotype of mice lacking functional deleted in colorectal cancer (Dec) gene. *Nature* **386**, 796–804 (1997).
16. T. Serafini, S. A. Colamarino, E. D. Leonardo, H. Wang, R. Beddington, W. C. Skarnes, M. Tessier-Lavigne, Netrin-1 is required for commissural axon guidance in the developing vertebrate nervous system. *Cell* **87**, 1001–1014 (1996).
17. C. Sabatier, A. S. Plump, M. Le, K. Brose, A. Tamada, F. Murakami, E. Y. Lee, M. Tessier-Lavigne, The divergent Robo family protein rig-1/Robo3 is a negative regulator of slit responsiveness required for midline crossing by commissural axons. *Cell* **117**, 157–169 (2004).
18. C. Laumonnerie, Y. G. Tong, H. Alstermark, S. I. Wilson, Commissural axonal corridors instruct neuronal migration in the mouse spinal cord. *Nat. Commun.* **6**, 7028 (2015).
19. P. Zelina, H. Blockus, Y. Zagar, A. Peres, F. Friocourt, Z. Wu, N. Rama, C. Fouquet, E. Hohenester, M. Tessier-Lavigne, J. Schweitzer, H. Roest Crollius, A. Chedotal, Signaling switch of the axon guidance receptor Robo3 during vertebrate evolution. *Neuron* **84**, 1258–1272 (2014).
20. A. Jaworski, I. Tom, R. K. Tong, H. K. Gildea, A. W. Koch, L. C. Gonzalez, M. Tessier-Lavigne, Operational redundancy in axon guidance through the multifunctional receptor Robo3 and its ligand NELL2. *Science* **350**, 961–965 (2015).
21. Y. Inamata, R. Shirasaki, Dbx1 triggers crucial molecular programs required for midline crossing by midbrain commissural axons. *Development* **141**, 1260–1271 (2014).
22. K. Keino-Masu, M. Masu, L. Hinck, E. D. Leonardo, S. S. Chan, J. G. Culotti, M. Tessier-Lavigne, Deleted in Colorectal Cancer (DCC) encodes a netrin receptor. *Cell* **87**, 175–185 (1996).
23. A. K. Dillon, S. C. Fujita, M. P. Matise, A. A. Jarjour, T. E. Kennedy, H. Kollmus, H. H. Arnold, J. A. Weiner, J. R. Sanes, Z. Kaprielian, Molecular control of spinal accessory motor neuron/axon development in the mouse spinal cord. *J. Neurosci.* **25**, 10119–10130 (2005).
24. G. Bai, O. Chivatakarn, D. Bonanomi, K. Lettieri, L. Franco, C. Xia, E. Stein, L. Ma, J. W. Lewcock, S. L. Pfaff, Presenilin-dependent receptor processing is required for axon guidance. *Cell* **144**, 106–118 (2011).
25. S. I. Wilson, B. Shafer, K. J. Lee, J. Dodd, A molecular program for contralateral trajectory: Rig-1 control by LIM homeodomain transcription factors. *Neuron* **59**, 413–424 (2008).
26. J. Bouvier, M. Thoby-Brisson, N. Renier, V. Dubreuil, J. Ericson, J. Champagnat, A. Pierani, A. Chedotal, G. Fortin, Hindbrain interneurons and axon guidance signaling critical for breathing. *Nat. Neurosci.* **13**, 1066–1074 (2010).
27. J. N. Murdoch, J. Eddleston, N. Leblond-Bourget, P. Stanier, A. J. Copp, Sequence and expression analysis of Nhlh1: A basic helix-loop-helix gene implicated in neurogenesis. *Dev. Genet.* **24**, 165–177 (1999).
28. K. Theodorakis, K. Kyriakopoulou, M. Wassef, D. Karagogeos, Novel sites of expression of the bHLH gene NSCL1 in the developing nervous system. *Mech. Dev.* **119**, S103–S106 (2002).
29. M. Kruger, T. Braun, The neuronal basic helix-loop-helix transcription factor NSCL-1 is dispensable for normal neuronal development. *Mol. Cell. Biol.* **22**, 792–800 (2002).
30. M. Kruger, K. Ruschke, T. Braun, NSCL-1 and NSCL-2 synergistically determine the fate of GnRH-1 neurons and control necdin gene expression. *EMBO J.* **23**, 4353–4364 (2004).
31. T. Schmid, M. Kruger, T. Braun, NSCL-1 and -2 control the formation of precerebellar nuclei by orchestrating the migration of neuronal precursor cells. *J. Neurochem.* **102**, 2061–2072 (2007).
32. D. Kawauchi, H. Taniguchi, H. Watanabe, T. Saito, F. Murakami, Direct visualization of nucleogenesis by precerebellar neurons: Involvement of ventricle-directed, radial fibre-associated migration. *Development* **133**, 1113–1123 (2006).
33. K. T. Yee, H. H. Simon, M. Tessier-Lavigne, D. M. O'Leary, Extension of long leading processes and neuronal migration in the mammalian brain directed by the chemoattractant netrin-1. *Neuron* **24**, 607–622 (1999).
34. J. A. Castro-Mondragon, R. Riudavets-Puig, I. Rauluseviciute, R. B. Lemma, L. Turchi, R. Blanc-Mathieu, J. Lucas, P. Boddie, A. Khan, N. Manosalva Perez, O. Fornes, T. Y. Leung, A. Aguirre, F. Hammal, D. Schmelter, D. Baranasic, B. Ballester, A. Sandelin, B. Lenhard, K. Vandepoele, W. W. Wasserman, F. Parcy, A. Mathelier, JASPAR 2022: The 9th release of the open-access database of transcription factor binding profiles. *Nucleic Acids Res.* **50**, D165–D173 (2022).
35. W. J. Kent, C. W. Sugnet, T. S. Furey, K. M. Roskin, T. H. Pringle, A. M. Zahler, D. Haussler, The human genome browser at UCSC. *Genome Res.* **12**, 996–1006 (2002).
36. R. J. Wingate, M. E. Hatten, The role of the rhombic lip in avian cerebellum development. *Development* **126**, 4395–4404 (1999).
37. J. Altman, S. A. Bayer, Development of the precerebellar nuclei in the rat: IV. The anterior precerebellar extramural migratory stream and the nucleus reticularis tegmenti pontis and the basal pontine gray. *J. Comp. Neurol.* **257**, 529–552 (1987).
38. D. Kawauchi, Y. Muroyama, T. Sato, T. Saito, Expression of major guidance receptors is differentially regulated in spinal commissural neurons transfated by mammalian Barh genes. *Dev. Biol.* **344**, 1026–1034 (2010).
39. C. G. Begley, S. Lipkowitz, V. Gobel, K. A. Mahon, V. Bertness, A. R. Green, N. M. Gough, I. R. Kirsch, Molecular characterization of NSCL, a gene encoding a helix-loop-helix protein expressed in the developing nervous system. *Proc. Natl. Acad. Sci. U.S.A.* **89**, 38–42 (1992).
40. L. Brown, R. Espinosa III, M. M. Le Beau, M. J. Siciliano, R. Baer, HEN1 and HEN2: A subgroup of basic helix-loop-helix genes that are coexpressed in a human neuroblastoma. *Proc. Natl. Acad. Sci. U.S.A.* **89**, 8492–8496 (1992).
41. L. Brown, R. Baer, HEN1 encodes a 20-kilodalton phosphoprotein that binds an extended E-box motif as a homodimer. *Mol. Cell. Biol.* **14**, 1245–1255 (1994).

42. E. Isogai, M. Ohira, T. Ozaki, S. Oba, Y. Nakamura, A. Nakagawara, Oncogenic LMO3 collaborates with HEN2 to enhance neuroblastoma cell growth through transactivation of Mash1. *PLOS ONE* **6**, e19297 (2011).
43. C. Manetopoulos, A. Hansson, J. Karlsson, J. I. Jonsson, H. Axelson, The LIM-only protein LMO4 modulates the transcriptional activity of HEN1. *Biochem. Biophys. Res. Commun.* **307**, 891–899 (2003).
44. D. J. Good, T. Braun, NHLH2: At the intersection of obesity and fertility. *Trends Endocrinol. Metab.* **24**, 385–390 (2013).
45. I. Sadowski, J. Ma, S. Triezenberg, M. Ptashne, GAL4-VP16 is an unusually potent transcriptional activator. *Nature* **335**, 563–564 (1988).
46. M. J. Fan, S. Y. Sokol, A role for Siamois in Spemann organizer formation. *Development* **124**, 2581–2589 (1997).
47. M. Placzek, J. Briscoe, The floor plate: Multiple cells, multiple signals. *Nat. Rev. Neurosci.* **6**, 230–240 (2005).
48. N. Bertrand, D. S. Castro, F. Guillemot, Proneural genes and the specification of neural cell types. *Nat. Rev. Neurosci.* **3**, 517–530 (2002).
49. D. J. Good, F. D. Porter, K. A. Mahon, A. F. Parlow, H. Westphal, I. R. Kirsch, Hypogonadism and obesity in mice with a targeted deletion of the Nhlh2 gene. *Nat. Genet.* **15**, 397–401 (1997).
50. T. Cogliati, D. J. Good, M. Haigney, P. Delgado-Romero, M. A. Eckhaus, W. J. Koch, I. R. Kirsch, Predisposition to arrhythmia and autonomic dysfunction in Nhlh1-deficient mice. *Mol. Cell. Biol.* **22**, 4977–4983 (2002).
51. J. Dodd, S. B. Morton, D. Karagogeos, M. Yamamoto, T. M. Jessell, Spatial regulation of axonal glycoprotein expression on subsets of embryonic spinal neurons. *Neuron* **1**, 105–116 (1988).
52. J. D. Comer, F. C. Pan, S. G. Willet, P. Haldipur, K. J. Millen, C. V. Wright, J. A. Kaltschmidt, Sensory and spinal inhibitory dorsal midline crossing is independent of Robo3. *Front. Neural Circuits* **9**, 36 (2015).
53. M. Barber, T. Di Meglio, W. D. Andrews, L. R. Hernandez-Miranda, F. Murakami, A. Chedotal, J. G. Parnavelas, The role of Robo3 in the development of cortical interneurons. *Cereb. Cortex* **19**, i22–i31 (2009).
54. M. Belle, D. Godefroy, C. Dominici, C. Heitz-Marchaland, P. Zelina, F. Hellal, F. Bradke, A. Chedotal, A simple method for 3D analysis of immunolabeled axonal tracts in a transparent nervous system. *Cell Rep.* **9**, 1191–1201 (2014).
55. M. Philipp, V. Niederkofler, M. Debrunner, T. Alther, B. Kunz, E. T. Stoeckli, RabGDI controls axonal midline crossing by regulating Robo1 surface expression. *Neural Dev.* **7**, 36 (2012).
56. A. Sagner, J. Briscoe, Establishing neuronal diversity in the spinal cord: A time and a place. *Development* **146**, (2019).
57. O. Avraham, Y. Hadas, L. Vald, S. Hong, M. R. Song, A. Klar, Motor and dorsal root ganglion axons serve as choice points for the ipsilateral turning of dI3 axons. *J. Neurosci.* **30**, 15546–15557 (2010).
58. J. P. Thaler, S. K. Lee, L. W. Jurata, G. N. Gill, S. L. Pfaff, LIM factor Lhx3 contributes to the specification of motor neuron and interneuron identity through cell-type-specific protein-protein interactions. *Cell* **110**, 237–249 (2002).
59. L. W. Jurata, S. L. Pfaff, G. N. Gill, The nuclear LIM domain interactor NLI mediates homo- and heterodimerization of LIM domain transcription factors. *J. Biol. Chem.* **273**, 3152–3157 (1998).
60. M. Bhati, C. Lee, A. L. Nancarrow, M. Lee, V. J. Craig, I. Bach, J. M. Guss, J. P. Mackay, J. M. Matthews, Implementing the LIM code: The structural basis for cell type-specific assembly of LIM-homeodomain complexes. *EMBO J.* **27**, 2018–2029 (2008).
61. O. Hobert, P. Kratsios, Neuronal identity control by terminal selectors in worms, flies, and chordates. *Curr. Opin. Neurobiol.* **56**, 97–105 (2019).
62. F. Friocourt, A. Chedotal, The Robo3 receptor, a key player in the development, evolution, and function of commissural systems. *Dev. Neurobiol.* **77**, 876–890 (2017).
63. K. Mukaigasa, C. Sakuma, H. Yaginuma, The developmental hourglass model is applicable to the spinal cord based on single-cell transcriptomes and non-conserved cis-regulatory elements. *Dev. Growth Differ.* **63**, 372–391 (2021).
64. J. Delile, T. Rayon, M. Melchionda, A. Edwards, J. Briscoe, A. Sagner, Single cell transcriptomics reveals spatial and temporal dynamics of gene expression in the developing mouse spinal cord. *Development* **146**, dev173807 (2019).
65. M. Haring, A. Zeisel, H. Hochgerner, P. Rinwa, J. E. T. Jakobsson, P. Lonnerberg, G. La Manno, N. Sharma, L. Borgius, O. Kiehn, M. C. Lagerstrom, S. Linnarsson, P. Ernfors, Neuronal atlas of the dorsal horn defines its architecture and links sensory input to transcriptional cell types. *Nat. Neurosci.* **21**, 869–880 (2018).
66. M. Shu, D. Hong, H. Lin, J. Zhang, Z. Luo, Y. Du, Z. Sun, M. Yin, Y. Yin, L. Liu, S. Bao, Z. Liu, F. Lu, J. Huang, J. Dai, Single-cell chromatin accessibility identifies enhancer networks driving gene expression during spinal cord development in mouse. *Dev. Cell* **57**, 2761–2775.e6 (2022).
67. A. Sathyamurthy, K. R. Johnson, K. J. E. Matson, C. I. Dobrott, L. Li, A. R. Ryba, T. B. Bergman, M. C. Kelly, M. W. Kelley, A. J. Levine, Massively parallel single nucleus transcriptional profiling defines spinal cord neurons and their activity during behavior. *Cell Rep.* **22**, 2216–2225 (2018).
68. V. Hamburger, H. L. Hamilton, A series of normal stages in the development of the chick embryo. *J. Morphol.* **88**, 49–92 (1951).
69. T. Shimizu, Y. Yamanaka, H. Nojima, T. Yabe, M. Hibi, T. Hirano, A novel repressor-type homeobox gene, ved, is involved in dharma/bozozok-mediated dorsal organizer formation in zebrafish. *Mech. Dev.* **118**, 125–138 (2002).
70. T. Sagai, T. Amano, A. Maeno, R. Ajima, T. Shiroishi, SHH signaling mediated by a prechordal and brain enhancer controls forebrain organization. *Proc. Natl. Acad. Sci. U.S.A.* **116**, 23636–23642 (2019).
71. L. Cong, F. A. Ran, D. Cox, S. Lin, R. Barretto, N. Habib, P. D. Hsu, X. Wu, W. Jiang, L. A. Marraffini, F. Zhang, Multiplex genome engineering using CRISPR/Cas systems. *Science* **339**, 819–823 (2013).
72. J. P. Concordet, M. Haeussler, CRISPOR: Intuitive guide selection for CRISPR/Cas9 genome editing experiments and screens. *Nucleic Acids Res.* **46**, W242–W245 (2018).
73. Y. Naito, K. Hino, H. Bono, K. Ui-Tei, CRISPRdirect: Software for designing CRISPR/Cas guide RNA with reduced off-target sites. *Bioinformatics* **31**, 1120–1123 (2015).
74. R. Ajima, E. Suzuki, Y. Saga, Pofut1 point-mutations that disrupt O-fucosyltransferase activity destabilize the protein and abolish Notch1 signaling during mouse somitogenesis. *PLOS ONE* **12**, e0187248 (2017).
75. M. Hashimoto, T. Takemoto, Electroporation enables the efficient mRNA delivery into the mouse zygotes and facilitates CRISPR/Cas9-based genome editing. *Sci. Rep.* **5**, 11315 (2015).
76. H. Nakamura, J. Funahashi, Introduction of DNA into chick embryos by in ovo electroporation. *Methods* **24**, 43–48 (2001).
77. K. Nishida, S. Matsumura, T. Kobayashi, Involvement of Brn3a-positive spinal dorsal horn neurons in the transmission of visceral pain in inflammatory bowel disease model mice. *Front. Pain Res.* **3**, 979038 (2022).
78. E. P. Consortium, J. E. Moore, M. J. Purcaro, H. E. Pratt, C. B. Epstein, N. Shoresh, J. Adrian, T. Kawli, C. A. Davis, A. Dobin, R. Kaul, J. Halow, E. L. Van Nostrand, P. Freese, D. U. Gorkin, Y. Shen, Y. He, M. Mackiewicz, F. Pauli-Behn, B. A. Williams, A. Mortazavi, C. A. Keller, X. O. Zhang, S. I. Elhajjajy, J. Huey, D. E. Dickel, V. Snetkova, X. Wei, X. Wang, J. C. Rivera-Mulia, J. Rozowsky, J. Zhang, S. B. Chhetri, J. Zhang, A. Victorsen, K. P. White, A. Visel, G. W. Yeo, C. B. Burge, E. Lecuyer, D. M. Gilbert, J. Dekker, J. Rinn, E. M. Mendenhall, J. R. Ecker, M. Kellis, R. J. Klein, W. S. Noble, A. Kundaje, R. Guigo, P. J. Farnham, J. M. Cherry, R. M. Myers, B. Ren, B. R. Graveley, M. B. Gerstein, L. A. Pennacchio, M. P. Snyder, B. E. Bernstein, B. Wold, R. C. Hardison, T. R. Gingeras, J. A. Stamatoyannopoulos, Z. Weng, Expanded encyclopaedias of DNA elements in the human and mouse genomes. *Nature* **583**, 699–710 (2020).
79. K. Katoh, D. M. Standley, MAFFT multiple sequence alignment software version 7: Improvements in performance and usability. *Mol. Biol. Evol.* **30**, 772–780 (2013).
80. K. Tamura, G. Stecher, S. Kumar, MEGA11: Molecular evolutionary genetics analysis version 11. *Mol. Biol. Evol.* **38**, 3022–3027 (2021).

Acknowledgments: We thank N. Yamatani, M. Yokoyama, and S. Noguchi for technical assistance; Y. Tanabe for *nls-EGFP* expression construct and the Isl1 antibody; M. Hibi for *VP16*- and *EnR*-containing plasmids; T. Shiroishi and T. Sagai for *Shh* riboprobe; A. Toyoda and H. Nakaoka for assistance on RNA-seq experiment; S. Kuraku for advice on phylogenetic analysis; and F. Murakami and Y. Hiromi for critical reading of the manuscript. We are grateful to A. Chédotal for discussions and communication of unpublished data. We would also like to thank Editage (www.editage.com) for English language editing. **Funding:** This study was funded by Grants-in-Aid for Scientific Research from the Ministry of Education, Culture, Science and Technology, Japan, contract grant numbers 16K07010, 20K06865, 23K05969 (Y.Z.), and 20H03345 (T.H.); and a grant from Israel Science Foundation, Israel, grant number 1787/21 (A.K.). **Author contributions:** Y.Z. conceived the study. A.M. and Y.Z. designed and conducted most of the experiments, analyzed data, and wrote the manuscript. K.N. performed the double-fluorescence ISH and the mouse spinal cord EP. R.A. and Y.S. generated the mutant mice. M.B. and A.K. identified the enhancer element, generated the in vivo reporter constructs, and performed the reporter analysis in chick. T.H. contributed materials and advices. Y.Z., A.K., and T.H. provided funding. All authors read and approved the manuscript. **Competing interests:** The authors declare that they have no competing interests. **Data and materials availability:** All data needed to evaluate the conclusions in the paper are present in the paper and/or the Supplementary Materials.

Submitted 14 August 2023
Accepted 16 April 2024
Published 23 May 2024
10.1126/sciadv.adk2149